MReadings: MR in RT

6th Edition ESTRO 2020

siemens.com/magnetom-world-rt

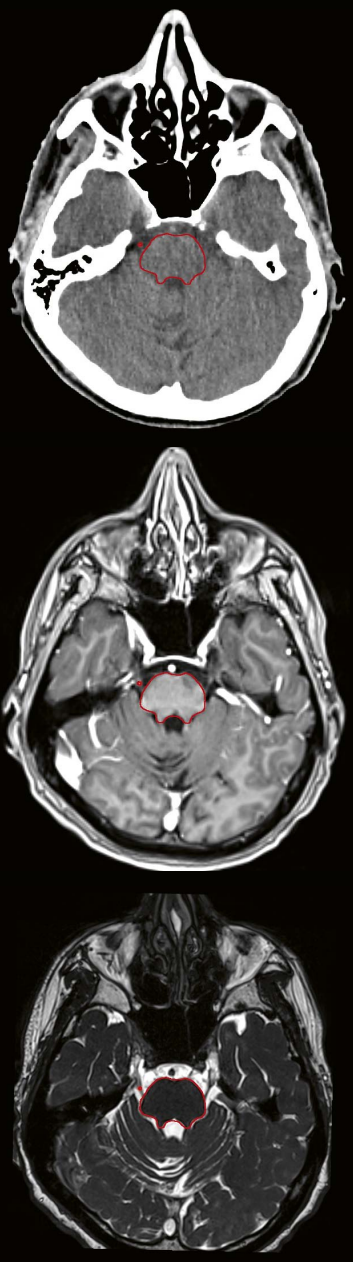

SIEMENS Healthineers

The entire editorial staff at MD Anderson Cancer Center and at Siemens Healthineers extends their appreciation to all the radiation oncologists, radiologists, technologists, physicists, experts, and scholars who donate their time and energy – without payment – in order to share their expertise with the readers of MAGNETOM Flash and the MReadings.

MAGNETOM Flash – Imprint

Publisher:
Siemens Healthcare GmbH
Magnetic Resonance,
Karl-Schall-Str. 6, D-91052 Erlangen, Germany

Editor-in-chief:
Antje Hellwich
(antje.hellwich@siemens-healthineers.com)

Guest Editor:
Caroline Chung, MD MSc FRCPC
Associate Professor,
Radiation Oncology & Diagnostic Imaging
Director of Imaging Technology & Innovation,
Radiation Oncology
The University of Texas MD Anderson Cancer Center,
Houston, Texas, USA

Editorial Board:
Rebecca Ramb, Ph.D.; Sunil Kumar S. L., Ph.D.;
Wellesley Were; Nadine Leclair, M.D.; Jane Kilkenny

Review Board:
Nuria Escobar Corral, Ph.D.; Elena Nioutsikou, Ph.D.;
Matthias Drobnitzky, Ph.D.; Daniel Fischer;
Glen Roberts

Copy Editing:
Sheila Regan, Jen Metcalf, UNIWORKS,
www.uni-works.org
(with special thanks to Kylie Martin)

Layout:
Agentur Baumgärtner,
Friedrichstr. 4, D-90762 Fürth, Germany

Production:
Norbert Moser,
Siemens Healthcare GmbH

Printer:
G. Peschke Druckerei GmbH,
Taxetstr. 4, D-85599 Parsdorf b. Munich, Germany

We welcome your questions and comments about the editorial content of MAGNETOM Flash. Please contact us at magnetomworld.team@siemens-healthineers.com

Manuscripts as well as suggestions, proposals and information are always welcome; they are carefully examined and submitted to the editorial board for attention. MAGNETOM Flash is not responsible for loss, damage, or any other injury to unsolicited manuscripts or other materials. We reserve the right to edit for clarity, accuracy, and space. Include your name, address, and phone number and send to the editors, address above.

MReadings: MR in RT is also available online:

www.siemens.com/magnetom-world-rt

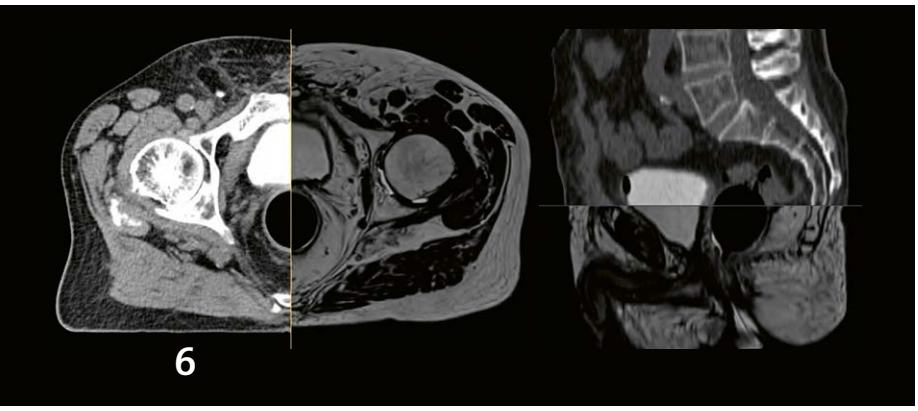

Advantages of acquiring the planning MRI in treatment position

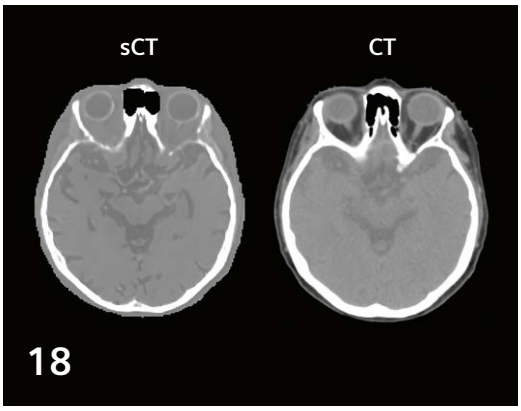

MR-only radiotherapy planning for brain tumors

Editorial Comment

Radiation Therapy

AI in MR

Meet Siemens Healthineers

[1]Work in progress: the application is currently under development and is not for sale in the U.S. and in other countries. Its future availability cannot be ensured.

Dr. Caroline Chung completed her undergraduate studies in biochemistry – molecular biology and genetics at the University of British Columbia (UBC) in Vancouver, Canada, in 1999 and continued at UBC to complete her medical degree and Radiation Oncology residency in 2008. She then completed a two year Research Fellowship in Radiation Oncology at the Princess Margaret Cancer Centre in Toronto, Canada, concurrently with a thesis M.Sc. at the University of Toronto's Institute of Medical Sciences and Royal College of Physicians and Surgeons of Canada Clinician Investigator Program at the University of British Columbia in 2011. Dr. Chung was then recruited to practice as a Clinician-Scientist in the Radiation Medicine Program of the Princess Margaret where she held the rank of Assistant Professor in the Department of Radiation Oncology at the University of Toronto and she was co-lead of the Brain Metastasis Clinic and Program at Princess Margaret Cancer Centre. In 2016, she was recruited to the MD Anderson Cancer Center in Houston, Texas, USA, to be the Director of the Advanced Imaging Strategic Initiative within the Division of Radiation Oncology with cross-appointment to Division of Diagnostic Imaging. She is currently an Associate Professor and the Director of Imaging Technology and Innovation within the Division of Radiation Oncology. In addition to running her own computational laboratory in oncological imaging research, as Director of Magnetic Resonance (MR) Research she leads collaborative research studies of MR-guided radiotherapy including the use of MR for target delineation, real-time MR image guidance

Advancing MR to Fulfil its Role in Oncology: Time to Finish the Pivot from Adjunctive to Essential

Dear readers and colleagues,

Cancer care has been transformed by the development of three-dimensional imaging techniques since their emergence into clinical care in the 1970s and 80s. Early computed tomography (CT) and magnetic resonance (MR) imaging systems provided soft-tissue visualization of both tumor and normal anatomy to provide oncologists with insights of the distribution and overall burden of disease that have advanced our ability to stage and prognosticate cancer since the first American Joint Committee Manual for Staging of Cancer in 1977 [1]. In those early days, imaging studies provided insights that were largely treated as qualitative, adjunctive information, which when combined with the clinical exam, would enhance clinical decision-making.

The role of imaging data in oncological clinical care has evolved dramatically in recent years where imaging has transitioned from its adjunctive role to become a clinician-directed measurement tool for prognostication and response assessment, as well as a tool for directly guiding intervention. MR imaging, in particular, has advanced at an astounding pace with improvements in image quality and new capabilities to interrogate tissue microstructure, physiology and metabolism, generating more mechanism-oriented measures that could be integrated into clinical decision-making for precision medicine approaches. However, while the imaging systems have advanced, the persistent qualitative nature in the use and interpretation of medical imaging has to-date prohibited utilizing the full potential of the rich multiparametric and multimodal imaging data in the guidance of cancer care.

Complementary to the advances in imaging technology itself, the rapidly growing computing power and prevalence of artificial intelligence (AI) in the world around us has certainly introduced new opportunities and challenges in medicine and particularly in the field of radiology. There are promising strides in utilizing AI to improve image quality, accelerate image acquisition and image reconstruction, as well as assist with image interpretation. One question that has arisen amidst the enthusiasm for AI applications in medical imaging is whether the requirements of imaging data are different in the adjunctive paradigm used by humans than numerical algorithms and whether the qualitative approach to imaging information in current practice will suffice in the era of human-machine hybrid medical care.

In order to fully address these evolving requirements and applications of imaging data, the community needs to make a conscious pivot from treating MR imaging data as a qualitative assessment tool when in actuality clinicians and the evolving technology around us are pushing its use as a quantitative measurement tool. This pivot requires critical steps that address the consistency and quality of imaging data at the time of imaging acquisition, post-processing and analysis, as well as changes in human behavior.

A dedicated effort is being led by groups including the Radiological Society of North America Quantitative Imaging Biomarker Alliance, which has broadly engaged institutions globally and partnered with industry to facilitate this transition of imaging from pictures to quantitative measurement. Through growing knowledge dissemination, clinical trial investigators have come to appreciate the impact of variable image acquisition on robust response assessment.

Work in progress: the application is currently under development and is not for sale in the U.S. and in other countries. Its future availability cannot be ensured.

of radiation delivery and imaging biomarkers of response. Her major research focus is in the utilization of advanced imaging to measure and predict response and toxicity to treatment. In her career, she has published over 90 articles in peer-reviewed journals and has been highly successful in securing peer-reviewed funding for both clinical trials and translational research. Her efforts extend from preclinical investigations of imaging response biomarkers utilizing multi-parametric MR imaging for conformal radiotherapy and anti-angiogenic therapy thru to translational research of imaging biomarkers in clinical trials for patients treated with SRS with and without anti-angiogenic therapy for brain metastases. She is a principal investigator in an NCI-supported randomized trial of bevacizumab vs. corticosteroids for brain radionecrosis that incorporated advanced MR for both trial eligibility and early response assessment. More recently, she has established collaborative projects with NASA to investigate imaging and fluid-based biomarkers of radiation injury to the heart and brain. Dr. Chung has also made significant contributions to the field through her work on standardization in medical imaging. She is co-chair of the Dynamic Contrast Enhanced-MRI Committee for the Radiological Society of North America Quantitative Imaging Biomarker Alliance, a member of the Jumpstarting Brain Tumor Drug Development Coalition's Imaging Standardization Steering Committee, Co-Chair of the Neuro-imaging Subcommittee in the Neuro-Oncology Committee of the Alliance for Clinical Trials in Oncology and has taken leadership in the development of quantitative imaging initiatives both in Toronto and Houston. She is active in the Radiation Oncology and Diagnostic Radiology communities in her dedicated efforts to advance the role of quantitative imaging and technology in cancer care, to develop gender diversity in leadership, and for her passion in supporting and supervising young talent.

Recently, members of collaborative clinical trial groups with the endorsement of the U.S. Food and Drug Administration (FDA) and National Cancer Institution (NCI) have established standardized MR acquisition protocols for primary and secondary brain tumors [2–4]. While establishing consensus for standardized image acquisition protocols are a first step, clinical adoption of these standardized protocols remains a challenge and along with this, the quality assessment metrics of MR imaging data need to be established for truly impactful implementation of quantitative MR imaging. Beyond the image acquisition, quantitative image interpretation also relies on standardized and transparent post-processing and analysis of imaging data with a quantitative approach, as fostered by groups such as the Quantitative Imaging Network [5–7]. Ideally, these academic collaborative efforts will include close industry engagement that will lead to the development of tools that enable broad deployment of quantitative MR implementation across varying clinical environments from large academic centers to community-based settings.

As highlighted in this edition of MReadings, the clinical research community is working aggressively to make the pivot and learn how to utilize the full and immense power of MR to quantitatively characterize and target tumors and tissues to improve radiotherapy delivery, as well as assess and adapt to early response to treatment. This transition will not only maximize the benefit of the ever-improving MR information to clinical decision-making, it will release the full power of multiparametric MR to characterize tissues for its use in biological targeting of tumor and biologically relevant radiation dosing of tumor subregions while limiting radiation-associated toxicity to the surrounding normal tissues – realizing personalized MR-guided radiotherapy.

Caroline Chung, MD MSc FRCPC
Associate Professor, Radiation Oncology & Diagnostic Imaging
Director of Imaging Technology & Innovation, Radiation Oncology
The University of Texas MD Anderson Cancer Center

References

1 Carr DT. The manual for the staging of cancer. Ann Intern Med. 1977;87(4):491-2. Epub 1977/10/01. doi: 10.7326/0003-4819-87-4-491. PubMed PMID: 907249.
2 Ellingson BM, Bendszus M, Boxerman J, Barboriak D, Erickson BJ, Smits M, Nelson SJ, Gerstner E, Alexander B, Goldmacher G, Wick W, Vogelbaum M, Weller M, Galanis E, Kalpathy-Cramer J, Shankar L, Jacobs P, Pope WB, Yang D, Chung C, Knopp MV, Cha S, van den Bent MJ, Chang S, Yung WK, Cloughesy TF, Wen PY, Gilbert MR, Jumpstarting Brain Tumor Drug Development Coalition Imaging Standardization Steering C. Consensus recommendations for a standardized Brain Tumor Imaging Protocol in clinical trials. Neuro Oncol. 2015;17(9):1188-98. Epub 2015/08/08. doi: 10.1093/neuonc/nov095. PubMed PMID: 26250565; PMCID: PMC4588759.
3 Goldmacher GV, Ellingson BM, Boxerman J, Barboriak D, Pope WB, Gilbert M. Standardized Brain Tumor Imaging Protocol for Clinical Trials. AJNR Am J Neuroradiol. 2015;36(10):E65-6. Epub 2015/09/12. doi: 10.3174/ajnr.A4544. PubMed PMID: 26359146.
4 Kaufmann TJ, Smits M, Boxerman J, Huang R, Barboriak DP, Weller M, Chung C, Tsien C, Brown PD, Shankar L, Galanis E, Gerstner E, van den Bent MJ, Burns TC, Parney IF, Dunn G, Brastianos PK, Lin NU, Wen PY, Ellingson BM. Consensus recommendations for a standardized brain tumor imaging protocol for clinical trials in brain metastases (BTIP-BM). Neuro Oncol. 2020. Epub 2020/02/13. doi: 10.1093/neuonc/noaa030. PubMed PMID: 32048719.
5 Press RH, Shu HG, Shim H, Mountz JM, Kurland BF, Wahl RL, Jones EF, Hylton NM, Gerstner ER, Nordstrom RJ, Henderson L, Kurdziel KA, Vikram B, Jacobs MA, Holdhoff M, Taylor E, Jaffray DA, Schwartz LH, Mankoff DA, Kinahan PE, Linden HM, Lambin P, Dilling TJ, Rubin DL, Hadjiiski L, Buatti JM. The Use of Quantitative Imaging in Radiation Oncology: A Quantitative Imaging Network (QIN) Perspective. Int J Radiat Oncol Biol Phys. 2018;102(4):1219-35. Epub 2018/07/04. doi: 10.1016/j.ijrobp.2018.06.023. PubMed PMID: 29966725; PMCID: PMC6348006.
6 Nordstrom RJ. The Quantitative Imaging Network in Precision Medicine. Tomography. 2016;2(4):239-41. Epub 2017/01/14. doi: 10.18383/j.tom.2016.00190. PubMed PMID: 28083563; PMCID: PMC5224526.
7 Clarke LP, Nordstrom RJ, Zhang H, Tandon P, Zhang Y, Redmond G, Farahani K, Kelloff G, Henderson L, Shankar L, Deye J, Capala J, Jacobs P. The Quantitative Imaging Network: NCI's Historical Perspective and Planned Goals. Transl Oncol. 2014;7(1):1-4. Epub 2014/04/29. doi: 10.1593/tlo.13832. PubMed PMID: 24772201; PMCID: PMC3998696.

MRI for Target Delineation in Radiotherapy – an Overview of Treatment Indications

Florian Putz, M.D.[1]; Thomas Weissmann, M.D.[1]; Veit Mengling, M.Sc.[1]; Rosalind Perrin, Ph.D.[1]; Siti Masitho, M.Sc.[1]; Johannes Rösch, M.D.[1]; Manuel Alexander Schmidt, M.D.[3]; Michael Uder, M.D.[2]; Rainer Fietkau, M.D.[1]; Christoph Bert, Ph.D.[1]

[1]Department of Radiation Oncology, Friedrich-Alexander-University Erlangen-Nuremberg, Erlangen, Germany
[2]Institute of Radiology, Friedrich-Alexander-University Erlangen-Nuremberg, Erlangen, Germany
[3]Department of Neuroradiology, Friedrich-Alexander-University Erlangen-Nuremberg, Erlangen, Germany

Abstract

Imaging used for target delineation and treatment planning plays a critical role for treatment success in radiotherapy. Due to its superior soft tissue contrast, MRI is essential for many radiotherapy treatment cases. In the present article, we summarize and discuss the role of MRI for the most relevant radiotherapy treatment indications.

Introduction

Radiotherapy has different demands on MR imaging than diagnostic radiology. In routine radiologic imaging, depending on the site and patient history, imaging primarily needs to be able to detect previously unknown pathologies and provide information on differential diagnosis while the accurate depiction of the true three-dimensional extension of tumors is of less importance. In contrast, MRI for radiotherapy planning primarily needs to accurately and clearly depict the tumor perimeter in three-dimensional space for precise gross tumor volume (GTV) delineation.

Different radiotherapy treatment indications and sites also may have specific demands on MR sequences and tissue contrasts. Frequently target delineation for treatment planning is based on contrast-enhanced T1 sequences. However, usually multiple tissue contrasts and sequences are integrated when creating target volumes for radiotherapy.

Magnetic resonance imaging is routinely required for treatment planning in many indications in radio-oncology [1]. In the present article we summarize the role of MRI for the most relevant radiotherapy treatment indications and discuss the varying specific requirements each treatment site puts on MR imaging.

Intracranial radiotherapy

One of the most important areas for MR imaging in radiotherapy are intracranial treatment indications. Intracranial targets, especially when small in size or low-enhancing, usually are not visualized on CT at all, rendering MR imaging critical for treatment planning. At the same time intracranial diseases are one of the most important indications for radiotherapy. Irradiation can be delivered very accurately to intracranial targets, as the skull can be positioned with submillimeter accuracy using thermoplastic mask immobilization and X-ray-based imaging during treatment delivery [2]. The high overall accuracy of intracranial radiotherapy enables precise target volumes and high radiotherapy doses with minimal impairment of normal tissues. This leads to high treatment efficacy and low or minimal side effects in a variety of malignant intracranial tumors like brain metastases, benign tumors like vestibular schwannoma and functional disorders like trigeminal neuralgia. In these diseases the requirements for geometric accuracy in MR imaging are particularly demanding, as commonly used margins of ≤ 1 mm do not account for additional MR imaging-related uncertainties [2, 3].

Another group of frequent intracranial treatment indications are gliomas, which are more difficult to treat as they are usually larger in size and show diffuse infiltration in the surrounding brain tissue, thus rendering precise delivery of high irradiation doses to all tumor cells is impossible without impairing normal brain tissue. In these tumors improved MR imaging could help with precise tumor delineation or potentially identifying candidate regions for dose-escalation and -sparing.

The concepts and information presented in this paper are based on research and are not commercially available.

Brain metastases

When being referred to treatment today, brain metastases are usually small (mostly < 1 cm diameter) solitary or multiple spherical lesions, which are best visualized in post-contrast T1 sequences. They show no or minimal infiltration into the surrounding brain tissue [4] and thus are usually irradiated with an isotropic uncertainty margin of less than 2 mm [2]. Due to the small size high-resolution isotropic 3D sequences are usually best-suited as they enable accurate multiplanar reconstruction and minimize partial volume effects [5, 6].

Inversion-recovery gradient echo sequences (IR-GRE) like the T1-MPRAGE [7], have been the most commonly used 3D MR imaging technique for brain tumors and have been included in the standardized Brain Tumor Imaging Protocol (BTIP) [8, 9]. However, multiple sources suggest that a 3D-turbo-spin-echo (TSE) T1-SPACE could be superior to the frequently used T1-MPRAGE gradient-echo sequence for intracranial radiotherapy target volume delineation [8, 10-12]. While T1-SPACE provides less contrast between grey and white matter [8], this is negligible in most cases for radiotherapy treatment planning and may in fact even help with the delineation of intracranial metastases, as does the suppression of vessels in the T1-SPACE [12]. Conversely, T1-MPRAGE suffers from a known reduced enhancement if low contrast agent uptake is present, which could lead to underestimation of lesion boundaries [8, 13] (Fig. 1).

Additional important requirements for radiotherapy in brain metastases are the minimization of distortions from gradient-non-linearities and susceptibility effect-induced distortions [14, 15].

Due to the malignant nature of brain metastases, they have a high growth rate [16, 17] and are usually surrounded by perifocal edema [18], which may change in configuration spontaneously or when corticosteroid dosage is modified (Fig. 2) [19]. Salkeld et al. found profound changes with imaging intervals ≤ 7 days before radiosurgery. Change in management was required for 41% of patients with interval ≤ 7 days and even for 78% if the delay exceeded 7 days. The most frequent reason for replanning was an increase in tumor or resection cavity size [17, 20]. Therefore, the interval between imaging and treatment delivery should be as short as possible. While same-day imaging would be optimal, in our university medical center in Erlangen we currently have established the requirement that the interval between imaging and treatment delivery must not exceed 5 days.

In addition to pretreatment changes, brain metastases may also undergo profound changes during radiotherapy due to transient swelling, changes in perifocal edema and treatment response (Fig. 2). Hessen et al. in a recent study evaluated the significance of a repeated MRI scan in the fractionated stereotactic radiotherapy of 18 brain metastases and 20 resection cavities. For cases with in-situ brain metastases, reductions in coverage of up

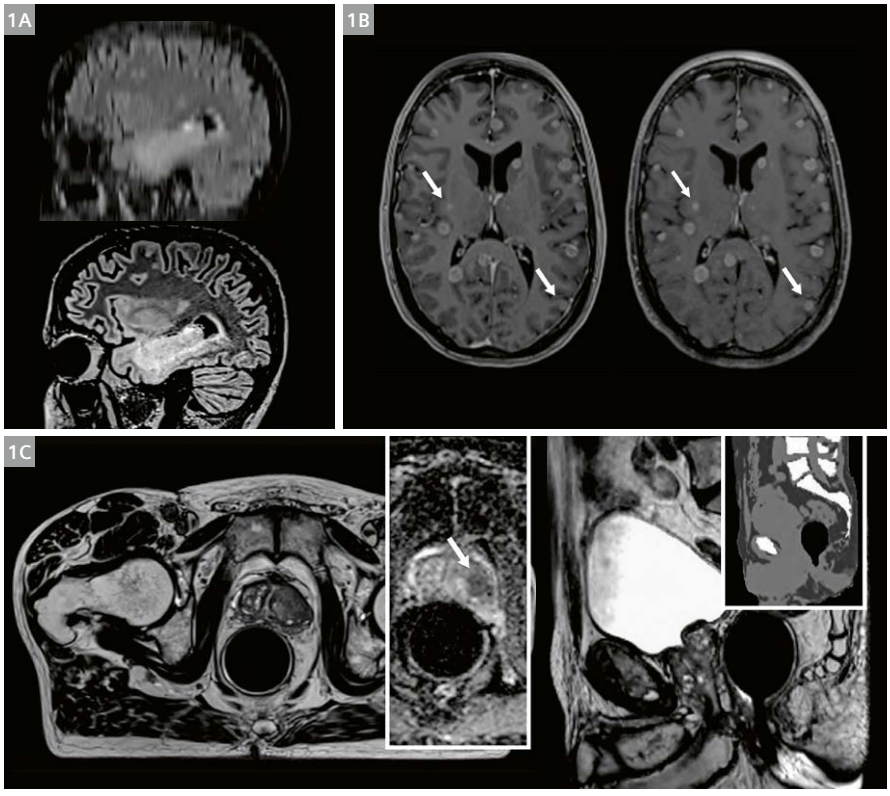

1 Examples of sequences used for target delineation.

(1A) T2 SPACE FLAIR (1 mm slice thickness – bottom) vs. conventional T2 FLAIR (5 mm slice thickness – top) in a patient with glioma.

(1B) T1 SPACE 3D TSE sequence (right) vs. T1 MPRAGE IR GE sequence (left). Some metastases are only very faintly visible in the T1 MPRAGE (arrows). Note also: Suppression of vessels and less contrast between gray and white matter in the T1-SPACE.

(1C) Isotropic T2 SPACE sequence in prostate cancer (left) with high-resolution sagittal reconstruction (right). Left inset: ADC map from diffusion-weighted imaging with reduced volume excitation (ZOOMit) showing focal diffusion restriction in the top lobe of the prostate (arrow). Right inset: Synthetic CT of the pelvis showing proper detection of air inside rectal balloon.

to 34.8% were found due to changes during fractionated radiotherapy [21].

This accumulating evidence for rapid tumor growth and accompanying anatomic changes in brain metastases might mean that optimal MR imaging for treatment planning needs to be performed daily. Considering the trend that more and more brain metastases are treated with stereotactic radiotherapy alone and life expectancies increase due to advances in immunotherapy and targeted agents [22], alternatives to contrast-enhanced T1 sequences might become necessary to reduce exposure to gadolinium-based contrast agents. Promising results recently have been achieved with deep learning-based prediction of synthetic contrast-enhanced T1 sequences from non-enhanced MR sequences, which could reduce cumulative gadolinium doses patients need to receive for radiotherapy [23].

There is a real potential for improving clinical outcomes with optimized MR imaging in brain metastases: In prospective clinical trials, local control rates of around 70% at 1 year post-radiotherapy have been consistently shown for stereotactic radiotherapy alone, while control rates for stereotactic radiotherapy with adjuvant whole brain radiotherapy measured at around 90% [24]. As increasing radiotherapy dose due to additional whole-brain radiotherapy is a less likely explanation, marginal miss in stereotactic radiotherapy because of suboptimal imaging could account for a substantial part of the observed difference in local efficacy.

Gliomas

While MRI was introduced many decades ago for target volume delineation in gliomas [25–28], these tumors are more difficult to treat and improvement in outcomes for the most part has stalled in recent years. Target delineation is more challenging in gliomas than in brain metastases. High-grade gliomas usually show strong contrast-enhancement, which is the main target for radiotherapy. However, while the surrounding T2 hyperintensity in brain metastases merely represents vasogenic edema and microscopic infiltration is minimal in brain metastases [4],

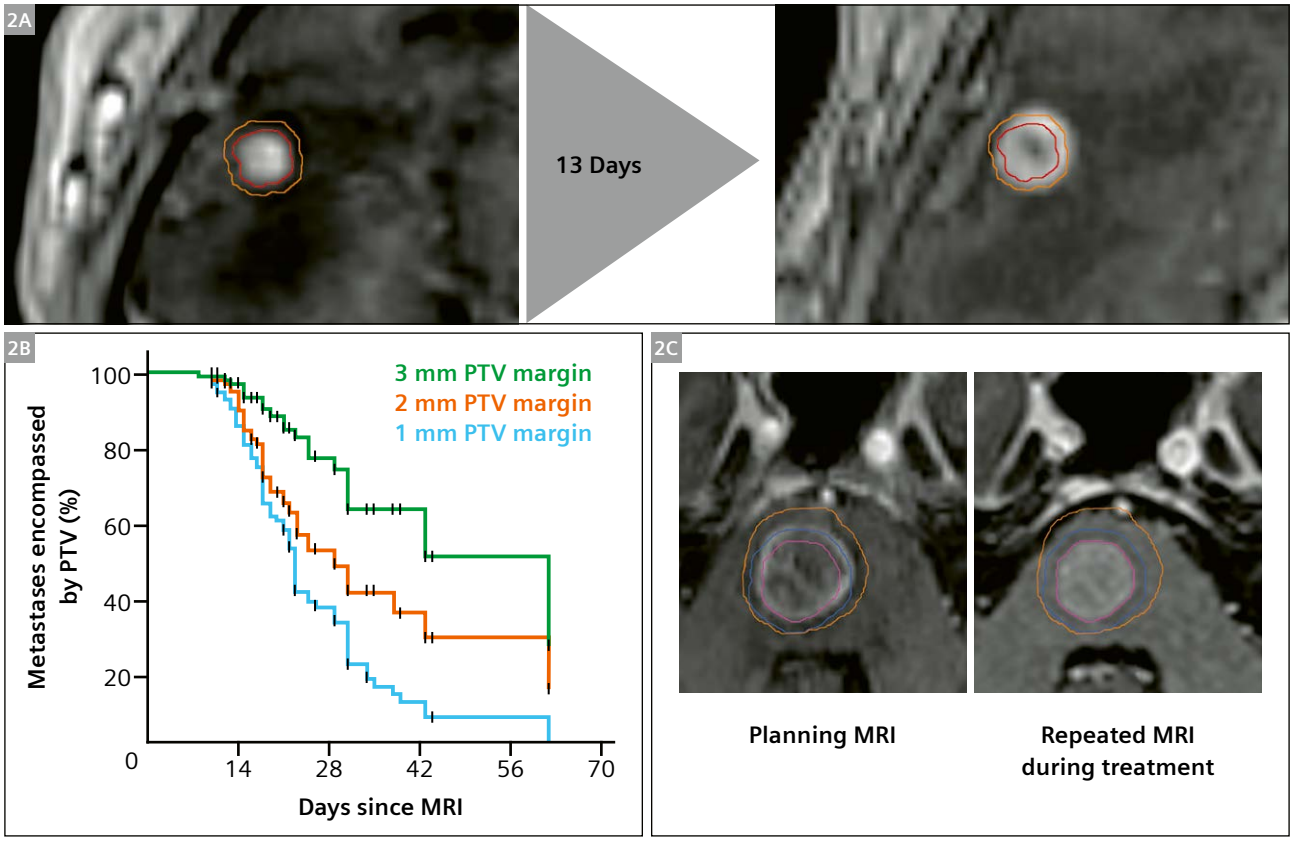

2 **Importance of the time interval between MR imaging and treatment delivery in brain metastases. (2A)** Brain metastasis increasing to 281% in volume in an interval of only 13 days. Orange: planning target volume (PTV) definition based on initial MRI would have missed 31.5% of GTV volume. **(2B)** Kaplan-Meier plot showing the diminishing fraction of metastases encompassed by the initial PTV volume over time for margin definitions of 1–3 mm (preliminary analysis of 85 metastases). **(2C)** Repeated planning MRI during fractionated stereotactic radiotherapy in a patient with brainstem metastasis. Note: Substantial reduction in tumor volume and in accompanying edema results in profound shifting of the brainstem. The radiotherapy plan was adapted based on the repeated planning MRI.

T2 abnormalities may constitute an important or the only visible tumor portion in low-grade gliomas or IDH-mutant glioblastomas [29–31].

Additionally, aside from imaging changes, extensive microscopic tumor cell infiltration into the adjacent brain is present in gliomas with microscopic infiltration even expected to extent into the contralateral brain hemisphere [32].

To make matters worse, contrast-enhancing tumor needs to be differentiated from treatment effects due to prior surgery and radiation as well as pseudo-progression.

For visualization of contrast-enhancing tumor, 3D contrast-enhanced T1-sequences like the T1-MPRAGE and T1-SPACE are usually used. In stark contrast to the millimeter margins employed in stereotactic radiotherapy for brain metastases, current guidelines recommend giving an isotropic margin of 2 cm around any contrast-enhancing tumor [29, 33]. Geometric accuracy therefore usually is less critical in radiotherapy for gliomas than in other intracranial treatment indications. The non-contrast enhancing tumor usually is delineated in 2D T2-FLAIR sequences with 3–5 mm slice thickness [34]. While current guidelines also recommend a margin of around 2 cm for T2-FLAIR hyperintensities in lower-grade gliomas, recommendations are conflicting in primary, IDH-wildtype, glioblastoma with the ESTRO recommending not considering the T2-FLAIR hyperintensity at all [29, 33].

As discussed above, thick slice 2D FLAIR sequences could lead to unnecessarily high treatment volumes in cases of small tumor volumes. Coarse depiction of non-enhancing tumor parts in conventional T2-FLAIR sequences should be of particular relevance in cases of stereotactic reirradiation, where much smaller margins are used.

We currently evaluate high-resolution 3D T2-SPACE FLAIR sequences in patients with malignant low-grade gliomas in comparison to conventional T2-FLAIR imaging. In our preliminary experience a 3D T2-SPACE FLAIR sequence allows for more precise delineation of non-enhancing tumor volumes with high-resolution multiplanar reconstruction being particularly beneficial to target delineation in radiotherapy (Fig. 1).

Moreover, RT-optimized perfusion and diffusion sequences could help with differentiating true tumor from other reasons for contrast-enhancement and T2-FLAIR hyperintensity. We are currently evaluating an EPI with reduced volume excitation (ZOOMit) to help with target volume delineation in gliomas.

Benign tumors and functional disorders

Vestibular schwannomas are an important benign tumor, frequently treated with stereotactic radiotherapy. In these cerebellopontine neoplasms excellent long-term control and functional outcome is achieved with local radiotherapy [35]. As vestibular schwannomas show strong contrast enhancement, 3D T1-sequences like the T1-MPRAGE are frequently used for delineation in radiotherapy treatment planning. In addition, high-resolution 3D-CISS sequences depict tumors and surrounding cerebrospinal fluid with high contrast and are important for delineation of adjacent cranial nerves. They also allow high-resolution segmentation of inner ear structures which may reduce cochlea doses and help with preservation of hearing. Post-radiotherapy these tumors frequently show transient enlargement before regressing in size, which sometimes is challenging to differentiate from treatment failure [35, 36].

Another benign brain tumor frequently treated with radiotherapy is meningioma, in which contouring mainly relies on contrast-enhanced T1 3D sequences like the T1-MPRAGE. In delineation of meningiomas for stereotactic radiotherapy the accurate estimation of the amount of dural extent (“Dural tail”) is frequently challenging to determine and contouring of meningioma cases is frequently very time-consuming because of complex geometric tumor configurations and imaging changes due to previous surgery.

Trigeminal neuralgia is a functional disorder that may be treated with stereotactic radiosurgery in patients refractory to analgesics and surgical decompression. A very large radiosurgery dose (70–90 Gy) is given to the trigeminal root entry zone or cisternal portion of the nerve making accurate high-resolution MRI for treatment planning crucial. We usually employ a high-resolution 3D CISS, which enables clear distinction of the trigeminal and surrounding cranial nerves [37].

Head and neck cancer

Radiotherapy of the head and neck region is a highly effective curative treatment for wide variety of tumors ranging from malignant entities like squamous cell cancers of the oral cavity and throat, malignant paranasal sinus tumors and lymphomas to benign indications like paraganglioma.

Substantial improvements in treatment side effects have been achieved with intensity-modulated radiotherapy (IMRT) by sparing of salivary glands, mucosal surfaces and skin [38]. By improving precision in tumor and lymph node level delineation, MR imaging for radiotherapy treatment planning has the potential to further reduce uncertainty margins and treatment side effects.

Important structures for radiotherapy planning in head and neck cancer show superior depiction in MRI compared to CT. These include salivary glands and cervical lymph nodes [39], but also malignant tissues. Rasch et al. observed that tumor volumes in advanced head and neck

cancer delineated in MRI are smaller and show less interobserver variability than using CT alone [40] and in nasopharyngeal cancer, Chung et al. showed in a study of 258 patients that MRI was far superior than CT for the detection of intracranial and pterygopalatine fossa invasion [41].

MRI for radiotherapy treatment planning in the head and neck region benefits greatly from image acquisition in treatment position as anatomic changes may become extensive, if the configuration of the cervical spine, mandible or scapula is different [1]. The anatomic changes usually are too large to be solved by non-rigid registration techniques with clinically desired accuracy [42]. Multiple groups therefore have developed solutions to acquire the MRI in treatment position with mask immobilization. A common challenge for acquiring MR studies in treatment position is that thermoplastic mask systems do not fit into routine head and neck coils. The most common solution therefore is to use flexible surface coils instead [1, 43, 44], with high-channel coils enabling decently good image quality.

Fat-saturated 3D post-contrast T1w-sequences are generally considered to be the backbone for radiotherapy target delineation [1, 43]. With 3D T2-FLAIR sequences and diffusion-weighted sequences providing additional information for delineation [43, 45].

Liver and abdominal tumors

Patients suffering from hepatic tumors can undergo a broad range of treatment options including surgery, radiofrequency ablation (RFA) and stereotactic body radiotherapy (SBRT). Large lesion size or close proximity to bigger vessels generally favor SBRT in comparison to RFA. A 2016 study published by Wahl et al. in the Journal of Clinical Oncology showed significantly improved tumor control for hepatocellular carcinoma treated with SBRT compared to RFA, if tumor diameter was ≥ 2 cm [46].

MR imaging is crucial for radiotherapy planning of hepatic tumors as the boundary of most lesions cannot be adequately discerned on CT and many tumors are not visible on CT at all.

Hepatic tumors usually show complex motion patterns during respiration as the liver not only undergoes movement but also deformation during the respiratory cycle and is additionally influenced by abdominal peristalsis [47, 48]. At the same time, uncertainty margins need to be minimized to spare surrounding liver and bowel while escalating radiotherapy dose to the target. Tumor motion and integration with the remaining SBRT workflow therefore are the main challenges in liver MRI for radiotherapy treatment planning.

Strategies for respiratory motion management in liver SBRT include internal target volume (ITV) concepts, expiration breath-hold, gating and tracking of tumor motion. As X-ray-based image guidance available at conventional linear accelerators does not visualize hepatic lesions, additional fiducials need to be invasively placed to allow for real-time image guidance. If radiotherapy is delivered exclusively in one respiratory phase, e.g. expiration, breath-hold or navigator-triggered MR sequences can be acquired to best reflect the respiratory position during treatment. As usual, MR imaging in radiotherapy treatment position using a flat table-top and similar immobilization equipment minimizes anatomic differences due to positioning. We currently use a navigator-triggered fat-saturated T2 TSE and EPI diffusion sequence as well as multiple breath-hold T1 VIBE Dixon sequences in different contrast phases for treatment planning.

4D MRI techniques are very promising for radiotherapy target volume delineation as they provide multiple 3D datasets during the respiratory cycle. 4D respiratory-correlated MRI acquires respiratory motion across multiple breathing cycles, which are subsequently sorted according to respiratory phase [49]. In contrast to 4D CT, 4D respiratory-correlated MRI thus provides data on an average breathing cycle that might be more representative of the actual respiration during treatment. 4D MRI datasets can be used to create an internal target volume, that encompasses all possible tumor positions and is treated in free-breathing, but it can also be exploited for expiration breath-hold, gating and tracking strategies that limit dose to surrounding structures. One limitation for tumor tracking on conventional linear accelerators is that only the position of the fiducial itself is tracked and changes in tumor shape and position in relation to the fiducials are not captured. An interesting method was published in 2018 by Harris et al. to use a pre-treatment 4D MRI together with LINAC on-board kV projections to generate a synthetic on-board 4D MRI on conventional linear accelerators [50]. Real-time image guidance of abdominal tumors is of course also a prime use case for new MR-LINAC systems and a technique for generating synthetic volumetric cine-MRI using the MR-LINAC on-board 2D-cine imaging as well as a pretreatment 4D MRI was developed by the same group before [51]. We currently acquire a transversal 4D T1 StarVIBE-based respiratory self-gating series with and without contrast in MRI simulation for liver SBRT reconstructing 5 to 7 respiratory bins. In our preliminary experience subtraction of pre- and postcontrast acquired 4D series further improves contrast ratio of target lesions.

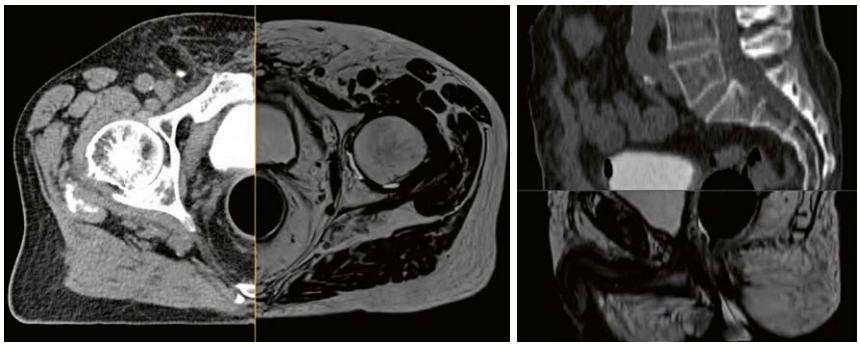

3 Advantages of acquiring the planning MRI in treatment position.
Planning MRI in prostate cancer showing good correspondence of bladder and rectum with endorectal balloon in the planning CT and dedicated planning MRI.

Prostate cancer

Prostate radiotherapy shows large benefits from MR imaging. Accurate delineation of the prostate is impossible in CT alone and it has been shown that prostate segmentations in CT are significantly larger than MRI, which leads to unnecessary high doses to penile and surrounding nerve and vascular structures and increases the risk for long-term urologic side effects [52, 53]. Precise radiotherapy delivery also reduces acute and late rectal side effects like proctitis. We therefore currently employ a rectal balloon and bladder filling protocol to enable a reliable anatomic configuration at each treatment session [53]. To assure accurate registration, we perform a dedicated MRI for radiotherapy treatment planning using the same positioning with rectal balloon and bladder filling as at daily treatment session. (Fig. 3) While a range of different non-rigid registration solutions are available, these algorithms may be associated with problematic uncertainties. For example, Brock et al. have observed errors of up to 8.7 mm for the prostate itself in intramodality non-rigid registration of repeated prostate MRIs [54]. As errors with non-rigid registration largely depend on the amount of deformation [7], performing MR measurements in treatment position also increases the accuracy of any subsequent registration steps.

We currently employ an isotropic, axial T2 SPACE with compressed sensing acceleration as the main sequence for delineation of the prostate, seminal vesicles and pelvic lymph nodes in patients with prostate cancer (Fig. 1). In our experience, this sequence provides high tissue contrasts, large field of view and allows for high-resolution sagittal reconstruction for differentiation of the caudal prostate margin and structures of the pelvic floor. As detailed sagittal imaging of the prostate and pelvic floor structures is of high importance in our experience, we currently still employ an additional sagittal T2 BLADE, which suppresses motion artifacts and provides high signal-to-noise in the prostate region. We use an EPI diffusion sequence with reduced volume excitation (ZOOMit) of the prostate region to get additional information on the location of malignant tumor inside the prostate (Fig. 1).

Summary

Optimal MR imaging for radiotherapy target delineation has distinct requirements that may be different from routine diagnostic indications. Demands on MR imaging in radiotherapy frequently are indication and site-specific, which needs to be addressed with specialized protocols. MRI for radiotherapy planning primarily needs to accurately and clearly depict the tumor perimeter in three-dimensional space for precise gross tumor volume delineation. In addition, 4D MRI techniques are capable of integrating tumor motion and have large potential to improve precision in radiotherapy of moving targets.

References

1 Paulson ES, Crijns SP, Keller BM, Wang J, Schmidt MA, Coutts G and van der Heide UA (2016) Consensus opinion on MRI simulation for external beam radiation treatment planning. Radiother Oncol 121 (2):187-192. doi:10.1016/j.radonc.2016.09.018

2 Kocher M, Wittig A, Piroth MD, Treuer H, Seegenschmiedt H, Ruge M, Grosu AL and Guckenberger M (2014) Stereotactic radiosurgery for treatment of brain metastases. A report of the DEGRO Working Group on Stereotactic Radiotherapy. Strahlentherapie und Onkologie: Organ der Deutschen Röntgengesellschaft [et al] 190 (6):521-532. doi:10.1007/s00066-014-0648-7

3 Shaw E, Scott C, Souhami L, Dinapoli R, Kline R, Loeffler J and Farnan N (2000) Single dose radiosurgical treatment of recurrent previously irradiated primary brain tumors and brain metastases: final report of RTOG protocol 90-05. Int J Radiat Oncol Biol Phys 47 (2):291-298.

4 Baumert BG, Rutten I, Dehing-Oberije C, Twijnstra A, Dirx MJ, Debougnoux-Huppertz RM, Lambin P and Kubat B (2006) A pathology-based substrate for target definition in radiosurgery of brain metastases. Int J Radiat Oncol Biol Phys 66 (1):187-194. doi:10.1016/j.ijrobp.2006.03.050

5 Anzalone N, Essig M, Lee SK, Dorfler A, Ganslandt O, Combs SE and Picozzi P (2013) Optimizing contrast-enhanced magnetic resonance imaging characterization of brain metastases: relevance to stereotactic radiosurgery. Neurosurgery 72 (5):691-701. doi:10.1227/NEU.0b013e3182889ddf

6 Snell JW, Sheehan J, Stroila M and Steiner L (2006) Assessment of imaging studies used with radiosurgery: a volumetric algorithm and an estimation of its error. Technical note. J Neurosurg 104 (1):157-162. doi:10.3171/jns.2006.104.1.157

7 Mugler JP, 3rd and Brookeman JR (1990) Three-dimensional magnetization-prepared rapid gradient-echo imaging (3D MP RAGE). Magnetic resonance in medicine 15 (1):152-157. doi:10.1002/mrm.1910150117

8 Danieli L, Riccitelli GC, Distefano D, Prodi E, Ventura E, Cianfoni A, Kaelin-Lang A, Reinert M and Pravata E (2019) Brain Tumor-Enhancement Visualization and Morphometric Assessment: A Comparison of MPRAGE, SPACE, and VIBE MRI Techniques. AJNR American journal of neuroradiology 40 (7):1140-1148. doi:10.3174/ajnr.A6096

9 Ellingson BM, Bendszus M, Boxerman J, Barboriak D, Erickson BJ, Smits M, Nelson SJ, Gerstner E, Alexander B, Goldmacher G, Wick W, Vogelbaum M, Weller M, Galanis E, Kalpathy-Cramer J, Shankar L, Jacobs P, Pope WB, Yang D, Chung C, Knopp MV, Cha S, van den Bent MJ, Chang S, Yung WK, Cloughesy TF, Wen PY and Gilbert MR (2015) Consensus recommendations for a standardized Brain Tumor Imaging Protocol in clinical trials. Neuro-oncology 17 (9):1188-1198. doi:10.1093/neuonc/nov095

10 Chappell PM, Pelc NJ, Foo TK, Glover GH, Haros SP and Enzmann DR (1994) Comparison of lesion enhancement on spin-echo and gradient-echo images. AJNR American journal of neuroradiology 15 (1):37-44.

11 Reichert M, Morelli JN, Runge VM, Tao A, von Ritschl R, von Ritschl A, Padua A, Dix JE, Marra MJ, Schoenberg SO and Attenberger UI (2013) Contrast-enhanced 3-dimensional SPACE versus MP-RAGE for the detection of brain metastases: considerations with a 32-channel head coil. Invest Radiol 48 (1):55-60. doi:10.1097/RLI.0b013e318277b1aa

12 Komada T, Naganawa S, Ogawa H, Matsushima M, Kubota S, Kawai H, Fukatsu H, Ikeda M, Kawamura M, Sakurai Y and Maruyama K (2008) Contrast-enhanced MR imaging of metastatic brain tumor at 3 tesla: utility of T(1)-weighted SPACE compared with 2D spin echo and 3D gradient echo sequence. Magnetic resonance in medical sciences: MRMS: an official journal of Japan Society of Magnetic Resonance in Medicine 7 (1):13-21. doi:10.2463/mrms.7.13

13 Mugler JP, 3rd and Brookeman JR (1993) Theoretical analysis of gadopentetate dimeglumine enhancement in T1-weighted imaging of the brain: comparison of two-dimensional spin-echo and three-dimensional gradient-echo sequences. Journal of magnetic resonance imaging: JMRI 3 (5):761-769. doi:10.1002/jmri.1880030512

14 Wang H, Balter J and Cao Y (2013) Patient-induced susceptibility effect on geometric distortion of clinical brain MRI for radiation treatment planning on a 3T scanner. Phys Med Biol 58 (3):465-477. doi:10.1088/0031-9155/58/3/465

15 Seibert TM, White NS, Kim GY, Moiseenko V, McDonald CR, Farid N, Bartsch H, Kuperman J, Karunamuni R, Marshall D, Holland D, Sanghvi P, Simpson DR, Mundt AJ, Dale AM and Hattangadi-Gluth JA (2016) Distortion inherent to magnetic resonance imaging can lead to geometric miss in radiosurgery planning. Practical radiation oncology 6 (6):e319-e328. doi:10.1016/j.prro.2016.05.008

16 Garcia MA, Anwar M, Yu Y, Duriseti S, Merritt B, Nakamura J, Hess C, Theodosopoulos PV, McDermott M, Sneed PK and Braunstein SE (2018) Brain metastasis growth on preradiosurgical magnetic resonance imaging. Practical radiation oncology 8 (6):e369-e376. doi:10.1016/j.prro.2018.06.004

17 Salkeld AL, Hau EKC, Nahar N, Sykes JR, Wang W and Thwaites DI (2018) Changes in Brain Metastasis During Radiosurgical Planning. Int J Radiat Oncol Biol Phys 102 (4):727-733. doi:10.1016/j.ijrobp.2018.06.021

18 Nardone V, Nanni S, Pastina P, Vinciguerra C, Cerase A, Correale P, Guida C, Giordano A, Tini P, Reginelli A, Cappabianca S and Pirtoli L (2019) Role of perilesional edema and tumor volume in the prognosis of non-small cell lung cancer (NSCLC) undergoing radiosurgery (SRS) for brain metastases. Strahlentherapie und Onkologie: Organ der Deutschen Röntgengesellschaft [et al] 195 (8):734-744. doi:10.1007/s00066-019-01475-0

19 Andersen C, Astrup J and Gyldensted C (1994) Quantitative MR analysis of glucocorticoid effects on peritumoral edema associated with intracranial meningiomas and metastases. Journal of computer assisted tomography 18 (4):509-518. doi:10.1097/00004728-199407000-00001

20 Scharl S, Kirstein A, Kessel KA, Duma MN, Oechsner M, Straube C and Combs SE (2019) Cavity volume changes after surgery of a brain metastasis-consequences for stereotactic radiation therapy. Strahlentherapie und Onkologie: Organ der Deutschen Röntgengesellschaft [et al] 195 (3):207-217. doi:10.1007/s00066-018-1387-y

21 Hessen E, Nijkamp J, Damen P, Hauptmann M, Jasperse B, Dewit L, Lutkenhaus L, Lamers E, van der Heide U, Damen E, Hanssens P and Borst G (2019) Predicting and implications of target volume changes of brain metastases during fractionated stereotactic radiosurgery. Radiother Oncol. doi:10.1016/j.radonc.2019.07.011

22 Badiyan SN, Regine WF and Mehta M (2016) Stereotactic Radiosurgery for Treatment of Brain Metastases. J Oncol Pract 12 (8):703-712. doi:10.1200/JOP.2016.012922

23 Kleesiek J, Morshuis JN, Isensee F, Deike-Hofmann K, Paech D, Kickingereder P, Kothe U, Rother C, Forsting M, Wick W, Bendszus M, Schlemmer HP and Radbruch A (2019) Can Virtual Contrast Enhancement in Brain MRI Replace Gadolinium?: A Feasibility Study. Invest Radiol 54 (10):653-660. doi:10.1097/rli.0000000000000583

24 Tsao M, Xu W and Sahgal A (2012) A meta-analysis evaluating stereotactic radiosurgery, whole-brain radiotherapy, or both for patients presenting with a limited number of brain metastases. Cancer 118 (9):2486-2493. doi:10.1002/cncr.26515

25 Potter R, Heil B, Schneider L, Lenzen H, al-Dandashi C and Schnepper E (1992) Sagittal and coronal planes from MRI for treatment planning in tumors of brain, head and neck: MRI assisted simulation. Radiother Oncol 23 (2):127-130. doi:10.1016/0167-8140(92)90344-t

26 Sumanaweera TS, Adler JR, Jr., Napel S and Glover GH (1994) Characterization of spatial distortion in magnetic resonance imaging and its implications for stereotactic surgery. Neurosurgery 35 (4):696-703; discussion 703-694. doi:10.1227/00006123-199410000-00016

27 Khoo VS, Dearnaley DP, Finnigan DJ, Padhani A, Tanner SF and Leach MO (1997) Magnetic resonance imaging (MRI): considerations and applications in radiotherapy treatment planning. Radiother Oncol 42 (1):1-15. doi:10.1016/s0167-8140(96)01866-x

28 Kondziolka D, Dempsey PK, Lunsford LD, Kestle JR, Dolan EJ, Kanal E and Tasker RR (1992) A comparison between magnetic resonance imaging and computed tomography for stereotactic coordinate determination. Neurosurgery 30 (3):402-406; discussion 406-407. doi:10.1227/00006123-199203000-00015

29 Niyazi M, Brada M, Chalmers AJ, Combs SE, Erridge SC, Fiorentino A, Grosu AL, Lagerwaard FJ, Minniti G, Mirimanoff RO, Ricardi U, Short SC, Weber DC and Belka C (2016) ESTRO-ACROP guideline "target delineation of glioblastomas". Radiother Oncol 118 (1):35-42. doi:10.1016/j.radonc.2015.12.003

30 Bynevelt M, Britton J, Seymour H, MacSweeney E, Thomas N and Sandhu K (2001) FLAIR imaging in the follow-up of low-grade gliomas: time to dispense with the dual-echo? Neuroradiology 43 (2):129-133. doi:10.1007/s002340000389

31 Buckner JC, Shaw EG, Pugh SL, Chakravarti A, Gilbert MR, Barger GR, Coons S, Ricci P, Bullard D, Brown PD, Stelzer K, Brachman D, Suh JH, Schultz CJ, Bahary JP, Fisher BJ, Kim H, Murtha AD, Bell EH, Won M, Mehta MP and Curran WJ, Jr. (2016) Radiation plus Procarbazine, CCNU, and Vincristine in Low-Grade Glioma. N Engl J Med 374 (14):1344-1355. doi:10.1056/NEJMoa1500925

32 Wang Y and Jiang T (2013) Understanding high grade glioma: molecular mechanism, therapy and comprehensive management.

Cancer letters 331 (2):139-146. doi:10.1016/j.canlet.2012.12.024

33 Gilbert MR, Wang M, Aldape KD, Stupp R, Hegi ME, Jaeckle KA, Armstrong TS, Wefel JS, Won M, Blumenthal DT, Mahajan A, Schultz CJ, Erridge S, Baumert B, Hopkins KI, Tzuk-Shina T, Brown PD, Chakravarti A, Curran WJ, Jr. and Mehta MP (2013) Dose-dense temozolomide for newly diagnosed glioblastoma: a randomized phase III clinical trial. Journal of clinical oncology: official journal of the American Society of Clinical Oncology 31 (32):4085-4091. doi:10.1200/jco.2013.49.6968

34 Menze BH, Jakab A, Bauer S, Kalpathy-Cramer J, Farahani K, Kirby J, Burren Y, Porz N, Slotboom J, Wiest R, Lanczi L, Gerstner E, Weber MA, Arbel T, Avants BB, Ayache N, Buendia P, Collins DL, Cordier N, Corso JJ, Criminisi A, Das T, Delingette H, Demiralp C, Durst CR, Dojat M, Doyle S, Festa J, Forbes F, Geremia E, Glocker B, Golland P, Guo X, Hamamci A, Iftekharuddin KM, Jena R, John NM, Konukoglu E, Lashkari D, Mariz JA, Meier R, Pereira S, Precup D, Price SJ, Raviv TR, Reza SM, Ryan M, Sarikaya D, Schwartz L, Shin HC, Shotton J, Silva CA, Sousa N, Subbanna NK, Szekely G, Taylor TJ, Thomas OM, Tustison NJ, Unal G, Vasseur F, Wintermark M, Ye DH, Zhao L, Zhao B, Zikic D, Prastawa M, Reyes M and Van Leemput K (2015) The Multimodal Brain Tumor Image Segmentation Benchmark (BRATS). IEEE transactions on medical imaging 34 (10):1993-2024. doi:10.1109/tmi.2014.2377694

35 Putz F, Muller J, Wimmer C, Goerig N, Knippen S, Iro H, Grundtner P, Eyupoglu I, Rossler K, Semrau S, Fietkau R and Lettmaier S (2017) Stereotactic radiotherapy of vestibular schwannoma: Hearing preservation, vestibular function, and local control following primary and salvage radiotherapy. Strahlentherapie und Onkologie: Organ der Deutschen Röntgengesellschaft [et al] 193 (3):200-212. doi:10.1007/s00066-016-1086-5

36 Mindermann T and Schlegel I (2014) How to distinguish tumor growth from transient expansion of vestibular schwannomas following Gamma Knife radiosurgery. Acta Neurochir (Wien) 156 (6):1121-1123. doi:10.1007/s00701-014-2063-3

37 Koca S, Distel L, Lubgan D, Lambrecht U, Bischoff B, Buchfelder M, Semrau S, Lettmaier S, Fietkau R and Putz F (2018) Time-course of pain response and toxicity after whole nerve encompassing LINAC-based radiosurgery for trigeminal neuralgia - a prospective observational study. Strahlentherapie und Onkologie: Organ der Deutschen Röntgengesellschaft [et al] In press

38 Saarilahti K, Kouri M, Collan J, Hamalainen T, Atula T, Joensuu H and Tenhunen M (2005) Intensity modulated radiotherapy for head and neck cancer: evidence for preserved salivary gland function. Radiother Oncol 74 (3):251-258. doi:10.1016/j.radonc.2004.11.004

39 Tien RD and Robbins KT (1992) Correlation of clinical, surgical, pathologic, and MR fat suppression results for head and neck cancer. Head & neck 14 (4):278-284. doi:10.1002/hed.2880140404

40 Rasch C, Keus R, Pameijer FA, Koops W, de Ru V, Muller S, Touw A, Bartelink H, van Herk M and Lebesque JV (1997) The potential impact of CT-MRI matching on tumor volume delineation in advanced head and neck cancer. Int J Radiat Oncol Biol Phys 39 (4):841-848. doi:10.1016/s0360-3016(97)00465-3

41 Chung NN, Ting LL, Hsu WC, Lui LT and Wang PM (2004) Impact of magnetic resonance imaging versus CT on nasopharyngeal carcinoma: primary tumor target delineation for radiotherapy. Head & neck 26 (3):241-246. doi:10.1002/hed.10378

42 Varadhan R, Karangelis G, Krishnan K and Hui S (2013) A framework for deformable image registration validation in radiotherapy clinical applications. Journal of applied clinical medical physics 14 (1):4066. doi:10.1120/jacmp.v14i1.4066

43 Mandija S, D'Agata F, Navest RJM, Sbrizzi A, Tijssen RHN, Philippens MEP, Raaijmakers CPJ, Seravalli E, Verhoeff JJC, Lagendijk JJW and van den Berg CAT (2019) Brain and Head-and-Neck MRI in Immobilization Mask: A Practical Solution for MR-Only Radiotherapy. Front Oncol 9:647. doi:10.3389/fonc.2019.00647

44 Wong OL, Yuan J, Yu SK and Cheung KY (2017) Image quality assessment of a 1.5T dedicated magnetic resonance-simulator for radiotherapy with a flexible radio frequency coil setting using the standard American College of Radiology magnetic resonance imaging phantom test. Quantitative imaging in medicine and surgery 7 (2):205-214. doi:10.21037/qims.2017.02.08

45 Cardoso M, Min M, Jameson M, Tang S, Rumley C, Fowler A, Estall V, Pogson E, Holloway L and Forstner D (2019) Evaluating diffusion-weighted magnetic resonance imaging for target volume delineation in head and neck radiotherapy. J Med Imaging Radiat Oncol 63 (3):399-407. doi:10.1111/1754-9485.12866

46 Wahl DR, Stenmark MH, Tao Y, Pollom EL, Caoili EM, Lawrence TS, Schipper MJ and Feng M (2016) Outcomes After Stereotactic Body Radiotherapy or Radiofrequency Ablation for Hepatocellular Carcinoma. Journal of clinical oncology: official journal of the American Society of Clinical Oncology 34 (5):452-459. doi:10.1200/jco.2015.61.4925

47 Akino Y, Oh RJ, Masai N, Shiomi H and Inoue T (2014) Evaluation of potential internal target volume of liver tumors using cine-MRI. Med Phys 41 (11):111704. doi:10.1118/1.4896821

48 Mostafaei F, Tai A, Omari E, Song Y, Christian J, Paulson E, Hall W, Erickson B and Li XA (2018) Variations of MRI-assessed peristaltic motions during radiation therapy. PloS one 13 (10):e0205917. doi:10.1371/journal.pone.0205917

49 Stemkens B, Paulson ES and Tijssen RHN (2018) Nuts and bolts of 4D-MRI for radiotherapy. Phys Med Biol 63 (21):21tr01. doi:10.1088/1361-6560/aae56d

50 Harris W, Wang C, Yin FF, Cai J and Ren L (2018) A Novel method to generate on-board 4D MRI using prior 4D MRI and on-board kV projections from a conventional LINAC for target localization in liver SBRT. Med Phys 45 (7):3238-3245. doi:10.1002/mp.12998

51 Harris W, Ren L, Cai J, Zhang Y, Chang Z and Yin FF (2016) A Technique for Generating Volumetric Cine-Magnetic Resonance Imaging. Int J Radiat Oncol Biol Phys 95 (2):844-853. doi:10.1016/j.ijrobp.2016.02.011

52 Rasch C, Barillot I, Remeijer P, Touw A, van Herk M and Lebesque JV (1999) Definition of the prostate in CT and MRI: a multi-observer study. Int J Radiat Oncol Biol Phys 43 (1):57-66. doi:10.1016/s0360-3016(98)00351-4

53 Bockelmann F, Hammon M, Lettmaier S, Fietkau R, Bert C and Putz F (2019) Penile bulb sparing in prostate cancer radiotherapy: Dose analysis of an in-house MRI system to improve contouring. Strahlentherapie und Onkologie: Organ der Deutschen Röntgengesellschaft [et al] 195 (2):153-163. doi:10.1007/s00066-018-1377-0

54 Brock KK (2010) Results of a multi-institution deformable registration accuracy study (MIDRAS). Int J Radiat Oncol Biol Phys 76 (2):583-596. doi:10.1016/j.ijrobp.2009.06.031

Contact

Dr. Florian Putz
Department of Radiation Oncology
Friedrich-Alexander-University Erlangen-Nuremberg
Universitaetsstraße 27
91054 Erlangen
Germany
Tel.: +49 9131 8534080
Fax: +49 9131 8534185
florian.putz@uk-erlangen.de

MR Imaging in Radiosurgery for Trigeminal Neuralgia

Aleksandra Grządziel[1]; Sławomir Blamek[2]; Barbara Bekman[1]; Sylwia Garbaciok[1]; Jacek Wendykier[1]; Krzysztof Ślosarek[1]

[1]Radiotherapy Planning Department, Maria Sklodowska-Curie National Research Institute of Oncology, Gliwice Branch, Gliwice, Poland
[2]Radiotherapy Department, Maria Sklodowska-Curie National Research Institute of Oncology, Gliwice Branch, Gliwice, Poland

Abstract

The hallmarks of radiosurgery for trigeminal neuralgia are high radiation doses, very small target volume, and close proximity to critical organs. This kind of treatment requires maximum precision in definition of all the anatomical structures. Although dose distribution is calculated with computed tomography, this modality alone cannot show specific anatomical volumes with sufficient precision. These discrete structures are clearly visible on various magnetic resonance imaging sequences. The highest possible accuracy of registration of CT images and specific MR sequences is vital. Our institutional protocol for all patients with intracranial lesions includes T1-weighted 3D MPRAGE without and with contrast enhancement. For trigeminal neuralgia cases, a CISS sequence is also routinely used. Thanks to its high-resolution imaging, the CISS sequence allows for accurate delineation of the target volume – the fifth cranial nerve – and organs at risk surrounding the target, including cranial nerves and the structures of the inner ear.

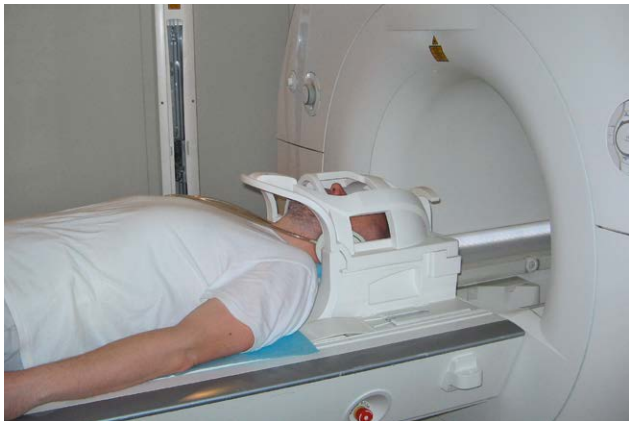

1 Patient examination position with head in Head/Neck 20 coil.

The Treatment Planning Department in the Maria Sklodowska-Curie National Research Institute of Oncology, Gliwice Branch, has been equipped with a 1.5T MAGNETOM Aera (Siemens Healthcare, Erlangen, Germany) since 2012. An on-site scanner is needed because MRI is used as a standard in both conventional radiotherapy and radiosurgical techniques. According to target volume type and location, various imaging sequences are routinely used.

Ionizing radiation has been successfully used for years in the treatment of trigeminal neuralgia. This method enables noninvasive treatment of severe facial pain using a high dose of radiation. With the Leksell Gamma Knife (Elekta AB, Stockholm, Sweden), high dose means 80–90 Gy in a single fraction specified at dose maximum. With the CyberKnife (Accuray, Sunnyvale, CA, USA), it means 60 Gy in a single fraction specified at the isodose encompassing the target volume [1–4]. High radiation doses, very small target volumes and close proximity to critical organs require definition of all the anatomical structures with the highest precision. With the CyberKnife system, the treatment planning calculation is performed with computed tomography (CT) data on electron density. However, CT imaging alone does not allow for differentiation of specific anatomical volumes, whereas these discrete structures are clearly visible on various MR sequences.

The accurate registration (also called fusion) of the planning CT and given MR sequence is vital. Registration in radiotherapy is a process of visualization and alignment of multimodal images [5, 6].

In our Institute, rigid registration is the standard method of handling diagnostic images used for radiotherapy planning. In case of trigeminal neuralgia, two different fusions are commonly used.

The concepts and information presented in this paper are based on research and are not commercially available.

Technical aspects of CT and MR scanning

Our routine practice is CT imaging in immobilization system with head mask. The CT scans are acquired from the top of the mask to the subclavian area. The CT image matrix resolution is 512 x 512 pixels with 1.0 mm gap between slices and 50 cm FOV acquired with 120 kV and 500 mAs. A flat scanner couch overlay is used for CT imaging to maintain the same position of the body as on the treatment couch.

The protocol for all patients with intracranial lesions includes T1-weighted 3D Magnetization Prepared Rapid Acquisition Gradient Echo (3D MPRAGE) without and with contrast enhancement. Moreover, for trigeminal neuralgia cases, a Constructive Interference in Steady State (CISS) sequence is routinely used [7–9]. This is a heavily T2-weighted fast gradient echo sequence of 0.35 mm spatial resolution. It allows for precise visualization of minute neural structures, especially the trigeminal nerve root where the target volume is located. Usually, one of two possible target volume locations is used. One is the root entry zone, close to the brainstem, allowing for excellent pain control [10], but irradiating this region is believed to be associated with higher rates of adverse effect, including facial hypoesthesia and anesthesia dolorosa. The second is the retrogasserian region (zona triangularis), which is more distant from the brainstem, and therefore thought to be safer to irradiate. The CISS sequence allows for accurate delineation of the target volume thanks to imaging with high resolution and great detail of the fifth cranial nerve against the background of bright cerebrospinal fluid. Moreover, it allows for accurate differentiation between nerve fibers and neighboring vessels, which are often the cause of trigeminal neuralgia due to neurovascular conflict.

Finally, it precisely reveals organs at risk surrounding the region of interest, including cranial nerves and the structures of the inner ear (cochlea and semicircular canals) [7]. To better identify vascular structures, especially if the cerebellopontine region has atypical anatomy, vascular sequences such as TOF (Time Of Flight) can be used.

MR scans are acquired with the patient positioned as in CT scanning, head first supine on a flat couch overlay (Fig. 1). The 3D MPRAGE sequence covers the entire head and a fragment of the cervical spine with 1 mm slices, with TR = 1390 ms and TE = 3.01 ms. The CISS sequence covers a slab of up to 10 cm of the head with the trigeminal nerve root located in the center. The CISS slice distance is 0.7 mm, with TR = 6.85 ms and TE = 3.43 ms.

The patient's position during MR scanning should be as close as possible to the position during the CT scan. This approach facilitates image registration and contouring, especially for the brainstem and medulla which can move significantly during flexion and extension of the neck.

Treatment planning aspects

The fusion of CT and MR images, regardless of the contouring and planning system, must be performed with care. Modern systems offer both automatic and manual rigid image registration. The planner must not rely solely on the automatic registration. Taking into account as many factors as possible during the image fusion is crucial in order to obtain the correct results. For CT/3D MPRAGE MR fusion, the anatomy of contrasted vessels, and the shapes of the brainstem and the medulla oblongata are analyzed. CT/CISS MR registration is performed taking into account the shapes of the brainstem, medulla, auditory nerve, and inner ear structures (Fig. 2).

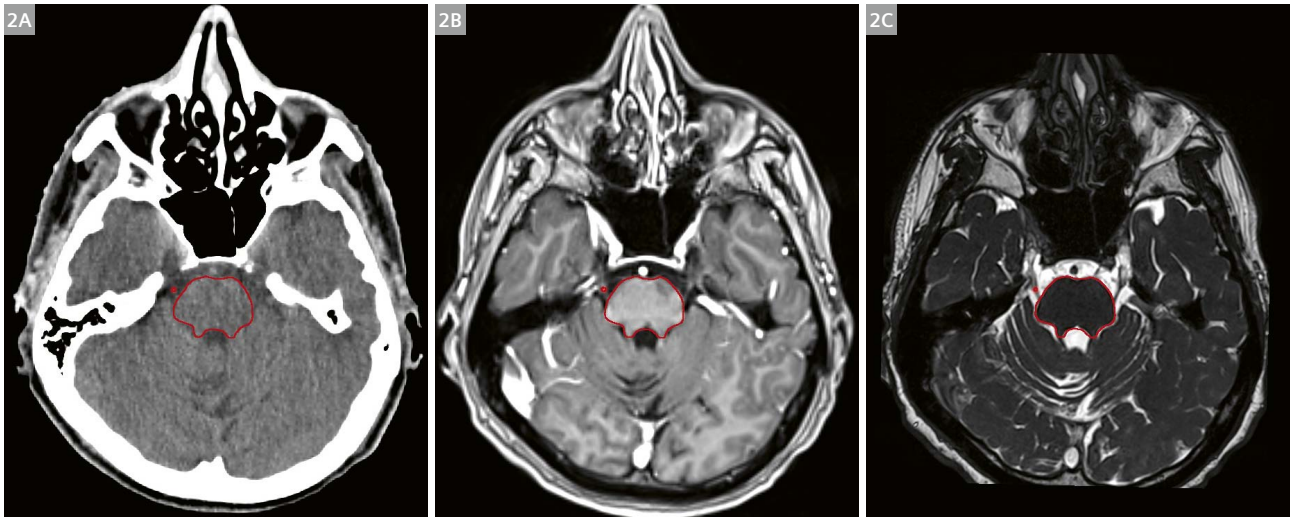

2 Transversal scans at the level of the target volume: **(2A)** CT with barely visible trigeminal nerve and brainstem; **(2B)** T1-weighted MPRAGE with barely visible trigeminal nerve, but well visible brainstem, **(2C)** T2-weighted CISS with clearly visible trigeminal nerve, brainstem and surrounding structures.

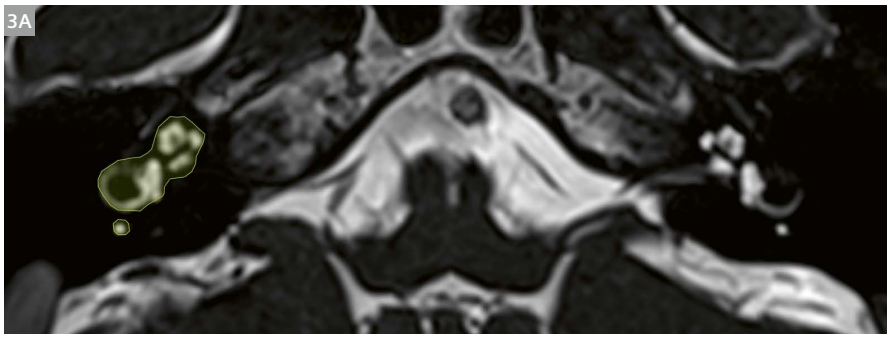

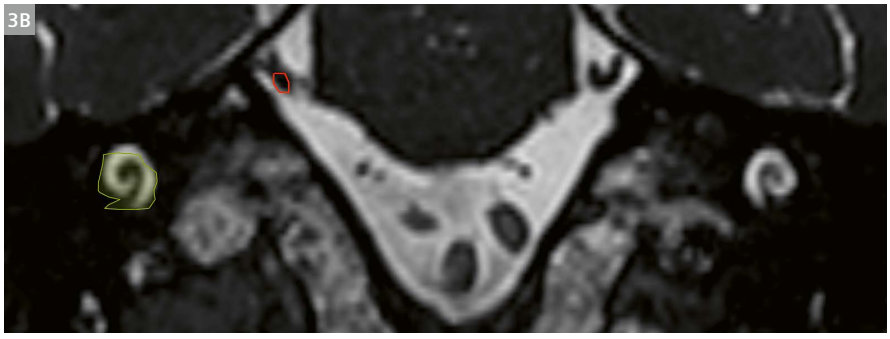

3 T2-weighted CISS in treatment planning system **(3A)** transversal image with contour of right inner ear structures (yellow), **(3B)** coronal image with contour of right cochlea (yellow) and trigeminal nerve (red).

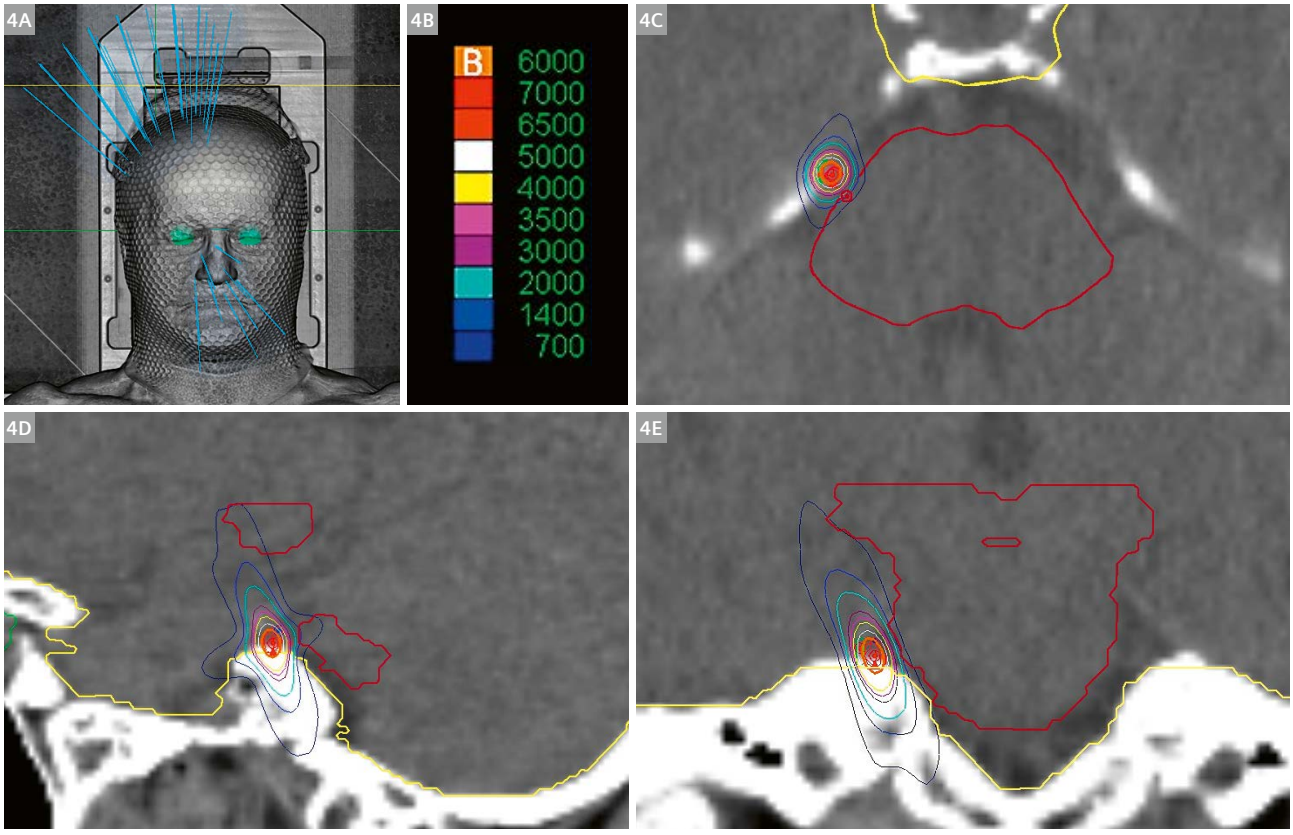

4 CyberKnife treatment plan for trigeminal neuralgia. **(4A)** 3D body surface reconstruction and beam arrangement, **(4B)** isocurve scale; structure delineation and dose distribution on the **(4C)** transversal, **(4D)** sagittal and **(4E)** coronal plane.

Delineation of the target and critical organs is done on CT images taking into account two fusions: the 3D MPRAGE and CISS sequences. The CISS sequence is the primary one for target and inner ear contouring (Fig. 3).

The goal of trigeminal neuralgia radiosurgery planning is to obtain a very high point dose in the target and a steep dose gradient outside the target where the nearest critical structures are located.

An acceptable plan must meet certain criteria for these critical structures, especially the brainstem but also the inner ear. In our center, for example, the dose delivered to the brainstem must not exceed 15 Gy and a dose of 10 Gy cannot be delivered in a volume larger than 0.5 cm^3. The doses in other critical structures farther from the target, such as the optic pathway, eyeballs, and lenses, are always monitored. Sparing organs at risk is a higher priority than target dose coverage.

Treatment plan evaluation requires careful reviewing of dose-volume histograms and CT scans one by one. It allows for controlling the dose distribution in the target area and capturing possible hotspots distant from the region of interest (Fig. 4).

Summary

Every year, more than a dozen trigeminal neuralgia treatments are performed at our Institute. CT imaging alone cannot show specific anatomical volumes with sufficient precision, but these small structures are more evident on different MR sequences. Therefore, it is essential to achieve the highest possible accuracy in registering of CT and specific MR sequences. Our institutional protocol for all patients with trigeminal neuralgia includes the registration of CT and 3D MPRAGE without and with contrast enhancement as well as a CISS sequence. Thanks to high resolution imaging, the CISS sequence allows for accurate delineation of the target volume i.e. the fifth cranial nerve, and organs at risk surrounding the target, including cranial nerves and the structures of inner ear. MR imaging is absolutely necessary as the base of exact target and critical structures delineation, allowing a high dose gradient in stereotactic plans to be achieved.

References

1 Niedzi L.A., The Implementation of Ablative Hypofractionated Radiotherapy for Stereotactic Treatments in the Brain and Body: Observations on Efficacy and Toxicity in Clinical Practice, Seminars in Radiation Oncology 18, 265-272 (2008).
2 Gorgulho A., Radiation mechanisms of pain control in classical trigeminal neuralgia, Surg Neurol Int. 3 Suppl 1, 17-25 (2012).
3 Obermann M., Treatment options in trigeminal neuralgia, Ther Adv Neurol Disord. 3 2, 107-115 (2010).
4 Mehrotra S.; Keane J.F.; Goldstain L., Trigeminal Neuralgia: Current Diagnosis and Treatment Options How to assess this debilitating chronic condition, which often mimics other disorders., Practical Pain Management 16 4, 46-47
5 Dogra A.; Goyal B.; Agrawal S., Medical Image Fusion: A Brief Introduction, Biomedical & Pharmacology Journal 11 3, 1209-1214 (2018).
6 James A.P.; Dasarthy B.V., Medical image fusion: A survey of the state of the art, Information Fusion 19, 4-19 (2014).
7 Chavhan G.B. et al., Steady-State MR Imaging Sequences: Physics, Classification, and Clinical Applications, RadioGraphics 28 4 (2008).
8 Elster A.D., Gradient-Echo MR Imaging: Techniques and Acronyms, Radiology 186, 1-8 (1993).
9 Hargreaves B.A., Rapid Gradient-Echo Imaging, Journal of Magnetic Resonance Imaging. 36, 1300-1313 (2012).
10 Somaza S.; Montilla E.M.; Mora M.C., Gamma knife radiosurgery on the trigeminal ganglion for idiopathic trigeminal neuralgia: Results and review of the literature, Surg Neurol Int. 10:89 (2019).

Contact

Professor Krzysztof Ślosarek
Radiotherapy Planning Department
Maria Sklodowska-Curie National Research Institute of Oncology
Gliwice Branch
15 Wybrzeże Armii Krajowej Street
44-101 Gliwice
Poland
Tel.: +32 278 88 86
onkologia@io.gliwice.pl

Clinical Implementation and Evaluation of MR-only Radiotherapy Planning for Brain Tumors

David Roberge, MD and Jean-Charles Côté, PhD

Department of Radiation Oncology, Centre Hospitalier de l'Université de Montréal (CHUM), Montreal, Canada

Introduction

Over the past decades, magnetic resonance (MR) imaging has been increasingly used to improve delineation of targets to be irradiated and organs at risk (OAR) to be avoided. In 2020, the list of clinical scenarios where MR is not considered useful is shorter than the list of sites where it is felt to provide benefit. This being said, for most uses of MR in radiotherapy planning, the level of evidence for clinical benefit is weak. Although it can often be demonstrated that physician segmentations will be altered by the use of MR, it is not often proven that these changes result in more cures or better quality of life. As adoption of MR planning increases, the quality of the evidence will likely improve.

An impediment to a more widespread use of MR in radiotherapy is the need to obtain both MR and CT images for treatment planning. In such a workflow the MR is used for tissue segmentation and the CT for treatment planning. In the combined workflow, image registration is required to align the images from both modalities. Target volumes and OARs defined in the MR image can then be transferred to the CT dataset, with which plan optimization and dose calculation are performed. The electron density information required for accurate dose calculation and reference images used for patient positioning are obtained from CT.

The challenges from a combined MR and CT workflow include:

- Accurate image registration between MR and CT. Small inaccuracies in registration will translate into systematic error throughout the treatment course.
- Patient scheduling. Scheduling patients on two different devices (CT and MR) can be burdensome on the patient and the healthcare institution. As time elapses between the images, anatomy can change (bladder filling as an example) and image registration may suffer.
- Financial issues. In bundled reimbursement schemes both imaging procedures may not be reimbursed presenting a burden to the institution. In schemes where both procedures are reimbursed, the additional imaging procedures and imaging devices represent a potentially unnecessary financial burden on the healthcare system as a whole.

An analogous situation existed after the introduction of CT simulation. Many patients underwent CT simulation followed by conventional fluoroscopic simulation. Today, most fluoroscopic simulators have been sold for scrap metal and, when necessary, digitally reconstructed radiographs are produced using CT images. A future can be imagined where CT scanners also disappear from radiation oncology departments.

In contrast to other disease sites, the use of MR for delineation in the management of brain tumors is not controversial. Many brain targets and organs at risk are

1 Example of patient positioning for MR Brain acquisition for radiation therapy planning on 1.5T MAGNETOM Aera.

simply not visible on CT – this is the case, for example, of small brain metastases and the hippocampal regions of the temporal lobes. In narrow indications, such as Gamma Knife radiosurgery, MR-only planning has been used in routine clinical practice for decades. This adoption of MR-only planning for frame-based radiosurgery has been facilitated by the absence of image-guidance, dose calculations which ignore tissue inhomogeneities and external MR fiducials which provide some measure of geometric quality assurance. In the more widespread implementation of MR-only planning, one must account for:

- Reference images for image guidance (CT or digitally reconstructed radiographs)
- Dose calculations which take into account electron density
- Quality assurance of the geometric integrity of varied MR images

Synthetic CT (sCT) provides images generated from MR scans that emulate CT images regarding electron density information and geometric representation. The images contain different Hounsfield units (HU) for different materials and these HU can be converted to electron density in the treatment planning system (TPS) using a calibration curve. The purpose of sCT images is to provide the same dose calculation accuracy as with CT images, enabling MR-only radiotherapy planning without needing additional CT images. Synthetic CT is now commercially available for both the brain and pelvis. After evaluating the pre-clinical version of this software, we have begun the clinical implementation of the commercial version and describe our experience herein.

Clinical workflow

The first step in the MR-only workflow is patient immobilization. In our workflow, the curved MR table is rendered flat using a custom insert. A commercial overlay is placed on the insert. In order to identify the treatment table in the treatment planning system, we lay a small slab of gel on the MR couch top. The patient lies on the table and is positioned straight using the sagittal in-room laser. The thermoplastic mask is heated outside the MR room and the warm mask impressionned on the patient. Although it is possible to use external fiducials or the laser bridge to mark an isocenter on the patient, we chose to use the tip of the nose as our reference. We feel that this is simple and accurate for our practice where every treatment fraction is preceded by a cone beam CT. Using an in-house plastic bridge, 2 flex small 4 coils are placed on each side of the head and a body 18 long above the patient. In addition, 2 rows of the spine 32 posterior coil are typically used for a total of 34 coil elements (Fig. 1).

For each clinical scenario, an MR protocol needs to be assembled around the sequences required for sCT. We chose to start our clinical implementation with whole-brain radiotherapy using hippocampal avoidance. This clinical scenario was chosen based on its incidence (not too common, not too rare), the low total dose and delivery via conventional linear accelerators. The MR protocol for this indication includes, in addition to localizer and quality assurance sequences, five sequences. The following sequences are required to generate sCT images of the brain: T1 VIBE Dixon, T2 SPACE, PETRA, FLASH Gradient Echo with "Time of Flight generated contrast" [2] (Fig. 2). For hippocampal avoidance an MPRAGE sequence is added.

The acquisition of the four sequences takes approximately 14 minutes on our MAGNETOM Aera[1] (1.5T) and is reported to last a similar time on a MAGNETOM Sola (1.5T) – 9 minutes with the MAGNETOM Vida (3T). We send the images to the hospital PACS and *syngo*.via. In *syngo*.via, the sCT image set is generated. Prior to being sent to our contouring server with the MPRAGE dataset, the sCT is inspected for aberrations or artefacts. The target and organs at risk are segmented by the physician before the case moves to dosimetry. The structure sets and images are sent to planning (in our case, this is the same platform as contouring) and the radiation plan is optimized.

Quality assurance

Once the images are acquired, the quality assurance sequences are reviewed for geometric accuracy quality control. For geometric quality assurance control, two sets of axial images are acquired in opposed frequency axis pushing the distortions each to one side. The bandwidth is reduced to amplify the distortion. The two sets of images are compared. The goal is to find distortion coming from the patient: surgical clip, dental implant, air, etc. Basic B_0 and gradients quality control are performed weekly on phantom and annually for exhaustive QC.

A first dosimetric quality assurance is performed by comparing plans with and without heterogeneity corrections before sending the plan to the linear accelerator. At the first treatment session, the sCT is visually compared to the cone-beam CT (CBCT). After the first treatment session, the dose is recalculated on the CBCT as a final quality control step.

[1] *MR protocols for Synthetic CT generation are works in progress for MAGNETOM Aera, they are currently under development and not for sale in the U.S. and in other countries. Their future availability cannot be ensured.*
MR protocols for Synthetic CT generation for 1.5T MAGNETOM Sola and 3T MAGNETOM Vida are clinically released.

Clinical implementation

In the process of clinical implementation, we chose to limit the use of sCT to a specific clinical scenario. In our clinic, the scenarios are formalized in radiation care plans – a total of approximately 30 for central nervous system cases and 40 for head and neck cases (without counting relevant palliative and lymphoma care plans). These care plans are made up of elements and are associated with various tasks. We modified the care plan for whole-brain radiotherapy with hippocampal avoidance to include sCT and the implementation was seamless for the physicians in our practice. In the process of implementation, the first patients had both an sCT and a conventional planning CT. Once we were comfortable that we had sampled the range of possible results (this required between 10 and 20 cases), the conventional CT was omitted.

Pitfalls

Although not specific to sCT, the distortion in the MR images is not uniform and will be greater near the sinuses. This does not have a significant impact in the care of patients with whole-brain radiotherapy but should be kept in mind for patients with lesions in or near the sinuses.

We have occasional cases in which a gel was used on the head support to increase patient comfort. This gel has led to unusual behavior of the sCT algorithm (Fig. 3) where bone is added between the patient and head support. This underlies the need to manually inspect all images. As well automatic segmentation tools which function on CT may not function on the sCT – this is the case of our automated brain segmentation tool.

Clinical evaluation of synthetic CT dose calculation accuracy

In our initial evaluation of the dose accuracy of patients treated with sCT, the clinical plan generated with the sCT is delivered virtually on the conventional CT and the dose compared through 3D subtraction and superimposed dose volume histograms.

Our observations after analyzing seven patients are that the derived dose is similar (typically within 2%) using sCT as compared to CT. The discrepancies seen result in slightly less dose being delivered to the patient – likely as a result of a thinner skull on the sCT.

Two case examples are illustrated in Figures 4 and 5. In the more favorable example, the mean target dose is within 0.1% and the minimum target dose within 2%. In an unfavorable case, the mean dose is still within 2% and the minimum dose within 4%. In both cases the direction of the discrepancies is the same with the patients likely receiving slightly less dose than planned.

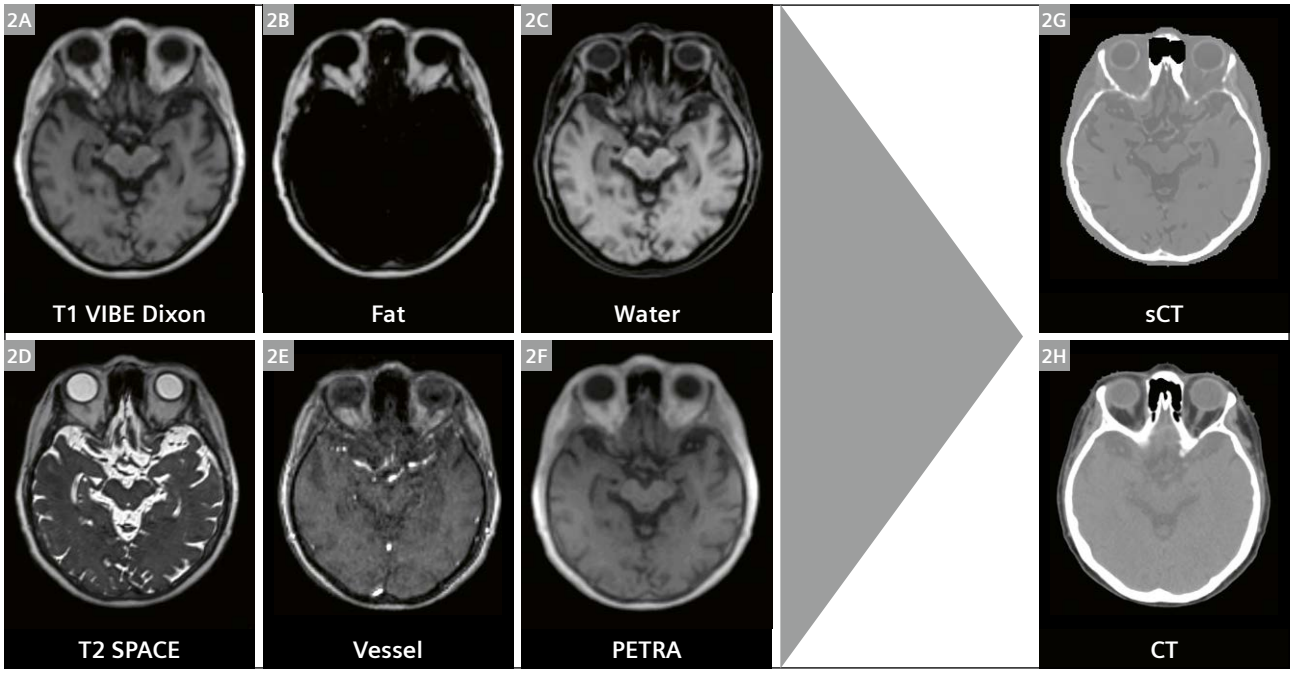

2 Image sets required to generate the sCT. The T1 VIBE Dixon sequence **(2A)** produces the fat and water images **(2B, C)** and the T2 SPACE sequence (**2D**, with an isotropic voxel size of 1 mm) is run to visualize the brain anatomy and morphology. The T2 SPACE sequence defines the resolution of the Synthetic CT output. The FLASH sequence **(2E)** is used to make sure that a vessel is not misclassified as bone and PETRA (**2F**, an ultra-short echo-time sequence sensitive to bone), is used as an override mask to correct voxels incorrectly identified as air.

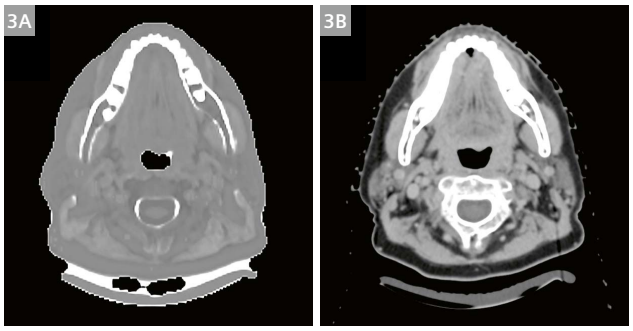

3 sCT artefact resulting from an immobilization device (**3A**: sCT and **3B**: CT).

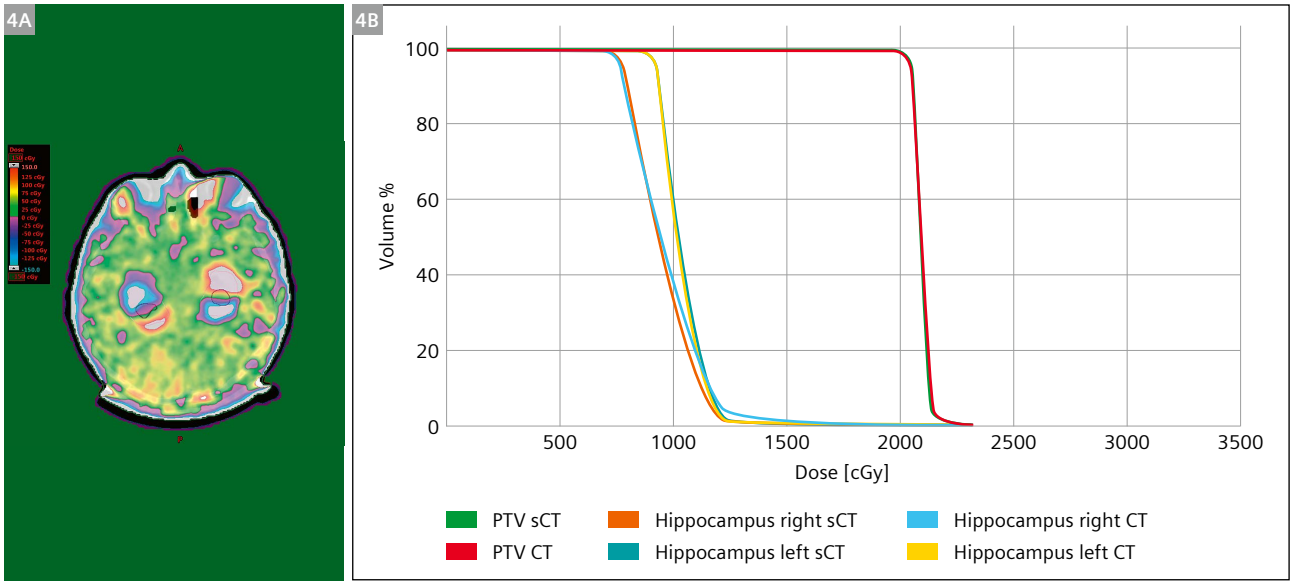

4 Dose subtraction and dose volume histograms from a clinical case.

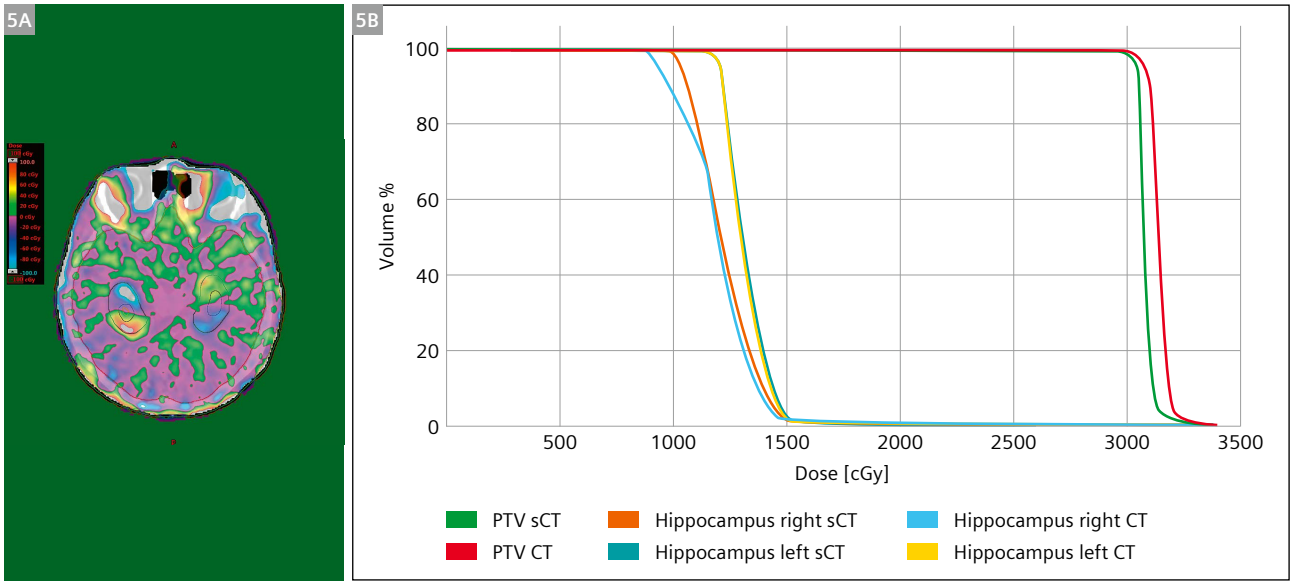

5 Dose subtraction and dose volume histograms from a clinical case.

Discussion

We have begun the clinical implementation of MR-only planning with the Siemens sCT protocol. Our preliminary evaluation is that this process allows a feasible and dosimetrically satisfactory workflow for whole-brain treatments. Our next step is to expand the use of this technology to other higher-dose brain treatments (high-grade gliomas are expected to be next). The MR-only workflow does add additional quality control steps which will hopefully be streamlines in the future. In the medium term, we plan to investigate the use of generative adversarial network (machine learning) generated images in an attempt to accelerate our workflow and improve accuracy.

References

1 Lorna Young et al., IMV Radiation Therapy Market Summary Report, Oct 2018.

2 SH Hsu et al., Investigation of a method for generating synthetic CT models from MRI scans of the head and neck for radiation therapy, Phys Med Biol. 2013 Dec 7;58(23):8419-35.

3 E Paradis et al., Assessing the dosimetric accuracy of MR-generated synthetic CT images for focal brain VMAT radiotherapy, Int J Radiat Oncol Biol Phys. 2015 Dec 1;93(5):1154-61.

4 SH Hsu et al., Quantitative Characterization of Ultrashort Echo (UTE) Images for supporting Air-Bone Separation in the Head, Phys Med Biol. 2015 Apr 7;60(7):2869-80.

5 Dr. Stéphane Muraro, Dr. Kinda Anna Saddi, White Paper: Simulation and data analysis in RT with *syngo*.via RT Image Suite, 2018.

6 Thian et al. Academic Radiology, 2014:21(4).

7 https://www.siemens-healthineers.com/de/magnetic-resonance-imaging/magnetom-world.

8 D Thorwarth et al., Synthetic CT Generation for the Pelvic Region Based on Dixon-MR Sequences: Workflow, dosimetric Quality and Daily Patient Positioning, 2018, MReadings: MR in RT, 5th Edition, ESTRO 2019:23-27.

9 DA Low et al, A technique for the quantitative evaluation of the dose distributions., Med Phys, 1998 May; 25(5):656-61.

Contact

Dr. David Roberge
Radiation Oncology
Centre Hospitalier de l'Université de Montréal (CHUM)
1000, rue Saint-Denis
Radio-oncologie, Pavillon C, C.S3.5002
Montreal QC H2X 0C1
Canada
Tel.: +1 514 890-8254
david.roberge.chum@ssss.gouv.qc.ca

Jean-Charles Côté, PhD David Roberge, MD

Put the advantages of the MAGNETOM World to work for you!

www.siemens.com/magnetom-world-rt

Siemens Healthineers' global MRI community offers peer-to-peer support and information. Radiation Oncologists, Radiologists, Medical Physicists, Technologists and Cardiologists have all contributed with publications, presentations, training documents, videos, case studies and more – all freely available to you via this unique network.

Don't miss the MRI protocols and practical tips and tricks for several body regions from experts for both experts and novice users. The information can help in supporting your entire clinical team and grow your practice.

The centerpiece of the MAGNETOM World Internet platform consists of MAGNETOM users' results. Here you will find articles, case reports and application tips allowing you to optimize your daily work.

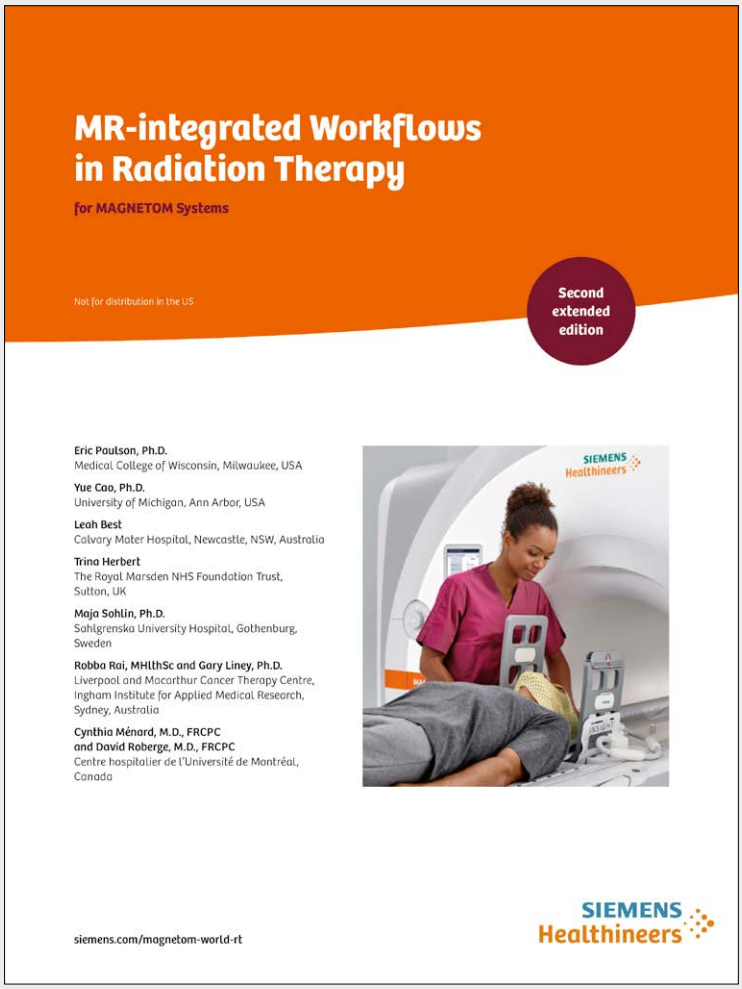

Clinical Implementation of MR-guided Radiotherapy for Prostate Cancer in Halcyon-System

Zimmermann M.[1]; Lange A.[2]; Sabatino M.[1]; Giro C.[1]; Lorenzen J.[3]; Struck J.[3]; Dahle J.[1]; Würschmidt F.[1]; Kretschmer M.[1]

[1]Radiologische Allianz, Strahlentherapie, Hamburg, Germany
[2]Beuth Hochschule für Technik, Berlin, Germany
[3]Radiologische Allianz, Diagnostische Radiologie, Hamburg, Germany

Introduction

In Germany, prostate cancer is the most common cancer among men. Approximately 58,000 men are diagnosed with prostate cancer each year, and more than 14,000 men die from it [1]. Almost half of all patients receive external beam radiotherapy (EBRT). Before treatment, a three-dimensional radiation therapy plan is created. Many clinics use thin-slice CT images to define the clinical target volume (CTV). Because of the limited soft tissue contrast of CT images, and the uncertainties in the treatment planning process, a large margin is needed to create the planning target volume (PTV). Early studies have shown that co-registered CT/MRI images improve target volume definition for radiotherapy planning of prostate cancer [2]. However, the image registration introduces an additional error in delineating targets and organs at risk (OARs) due to the modified geometry by two different examinations at two different time points.

A workflow based only on MR images (MR-only workflow)[1] offers considerably improved soft tissue contrast for CTV definition and improved OAR delineation without

Case	Age [years]	Weight [kg]	Gleason score	iPSA [ng/ml]	TNM
1	76	92	3 + 3 = 6	10.25	cT2a cN0 M0
2	78	85	5 + 4 = 9	6.50	cT2a cN0 cM0
3	78	84	3 + 3 = 6	32.80	pT3b pN0 (0/18) R1 Pn1 cM0
4	82	95	4 + 5 = 9	88.61	cT2b-c cN0 cM0
5	58	–	4 + 4 = 8	5.70	cT2c cN0 cM0
6	79	82	4 + 5 = 9	12.70	cT2c cN0 cM0
7	75	87	4 + 3 = 7	9.53	cT2c cN0 cM0
8	77	86	3 + 3 = 6	7.80	cT2b cN0 cM0
9	80	72	4 + 3 = 7	42.00	cT2c cN0 M1
10	68	83	3 + 4 = 7	9.45	pT1b pN0 cM0
11	72	84	5 + 4 = 9	11.00	cT2c cN0 cM0 Pn1
12	67	80	3 + 4 = 7	–	cT1c
13	71	72	3 + 4 = 7	101.00	pT3a pN0 (0/6) cM0 L0 V0 pM1 R1
14	74	85	4 + 5 = 9	6.58	cT2 cN0 cM0 pn1, G3
15	67	115	4 + 3 = 7	8.00	pT3b pN0 (0/5) L0 V0 Pn1 R1

Table 1: Clinical profile and tumor stages of the patients included in the implementation phase. Patients 6, 11, and 14 received radiation therapy to their lymph nodes.

registration errors. The acquisition and maintenance price is higher than that of CT imaging, but it can be considerably reduced by shared-use models including diagnostic radiology departments, so diagnostic images and MR-only sequences can be acquired in one session.

Optimizing the dose distribution requires electron density (or mass density), which is not provided by MR images. Moreover, modern image-guided radiotherapy (IGRT) linear accelerators need CT images as a reference to compare cone beam CT (CBCT) images with planning CT images for patient position correction before each treatment session. For these reasons synthetic CTs (sCT) have been introduced into clinical routine. Tissue classification methods as well as atlas-based and machine learning algorithms are used to generate sCT datasets from MR sequences. These algorithms have moved in recent years from research to the clinical world (so far for brain and pelvis cases). Commercially available solutions use somewhat different methods to generate the sCT images, and come with different business models. Spectronic offers a cloud-based pay-per-use approach, whereas Siemens Healthineers offers a classic software license model.

The main objective of our analysis was clinical implementation of the MR-only workflow in a novel ring-gantry linear accelerator system (Halcyon; Varian, Palo Alto, CA, USA) with daily CBCT based IGRT. We discuss in particular how daily CBCT guided IGRT based on sCT images compares with the traditional approach using a planning CT (pCT) image as reference. Detailed dose calculations are part of the comparison and complete the discussion.

Materials and methods

The implementation phase of MR-only radiotherapy took place from May to August 2019. It included all prostate patients without contraindications (such as pacemakers, extensive endoprosthesis, claustrophobia). During the consent discussion, patients were required to follow an empty rectum protocol before each imaging and treatment session. For radiotherapy planning, patients received first a planning CT scan with virtual simulation, and immediately afterwards (within a maximum of 30 minutes) an MRI scan in identical position.

1. Patient collective

In total 15 patients with different tumor stages were included in this study: 11 patients with localized tumors (T1–2, N0, M0), three patients with locally advanced tumors (T3a–T3b, N0, M0) and one patient with metastasis to the sacrum. Twelve of the patients included in this study received radiotherapy as primary therapy, and the other three received postoperative radiotherapy. Because of their PSA values and Gleason scores, three of the patients also had radiation therapy to their lymph nodes (Table 1).

2. CT/MRT virtual simulation

For pCT imaging, the SOMATOM Definition AS (Siemens Healthcare, Forchheim, Germany) with a slice thickness of 2 mm, 120 kV and iterative image reconstruction was used.

As MRI simulator, the 1.5T MAGNETOM Aera (Siemens Healthcare, Erlangen, Germany) installed in our clinic. Images are reconstructed with 2.5 mm slice thickness was used. Table 2 shows the acquired sequences.

For simulation purposes, patients must be scanned in the same position as on the treatment couch of the linear accelerator. So in the MRI scanner patients were positioned on a flat tabletop overlay using a knee immobilization device, reproducing the positioning setup during pCT imaging and during the treatment with the Halcyon system.

Figure 1 shows the body coil (Body 18 long MR coil 1.5T) fixed in place with a coil positioning aid (INSIGHT Body Coil Holder; Qfix, Avondale, PA, USA).

In addition to the diagnostic images (sequences listed in Table 2), the T1- and T2-sequences, together with the generated sCT are imported into the oncology information system (OIS) ARIA (Varian, Palo Alto, CA, USA). Contouring of the target volumes is performed on the images obtained from these sequences, using the diagnostic findings recorded in ARIA as support. The workflow is integrated into the ARIA CarePath.

Step	Sequence	Time in min
Orientation	localizer bh	00:17
	localizer @center	00:17
Overview	t2 tse sag 3.5 mm	04:30
	t2 haste cor mbh	00:49
Diffusion	ep2d diff b50 800 1400 tra 3 mm	04:36
sCT Spectronic	t2 tse tra p2 2.5 mm	13:35
sCT Siemens	t1 sCTp1-Dixon	02:32
Perfusion with KM	t1 vibe tra dyn 4 mm	02:05
	t1 fl2d fs tra mbh	01:20
Total		**30:17**

Table 2: Description of sequences used.

[1]*MR protocols for Synthetic CT generation are works in progress for MAGNETOM Aera, they are currently under development and not for sale in the U.S. and in other countries. Their future availability cannot be ensured. MR protocols for Synthetic CT generation for 1.5T MAGNETOM Sola and 3T MAGNETOM Vida are clinically released.*

3. Generation of sCT

3.1 Pay-per-use model (Spectronic)

Spectronic (Helsingborg, Sweden) uses an atlas-based algorithm for sCT image generation, offered as a cloud-based service[2]. Anonymized MRI datasets are transferred from PACS or directly from the MRI scanner to the cloud using a DICOM-receiver installed at the clinic network. After being de-anonymized in the DICOM-receiver the generated sCTs are transferred to PACS. Customers are informed by E-mail that new data are available. The sCT images are generated using a statistical decomposition algorithm (SDA) [3]. The atlas-based method is combined with machine learning. The algorithm calculates the most probable CT representation for an MRI image set, according to previously acquired datasets. So it is important always to follow the same protocol and use the same scan parameters when scanning patients, to obtain the same contrast as in the training datasets.

3.2 License-based model (Siemens Healthineers)

Siemens Healthineers combines a tissue classification and an atlas-based method to generate the sCT image. From the required T1 VIBE Dixon sequence, four MR datasets with different weighting in water, fat, in-phase and opposed-phase were obtained. The four sets or image sets are used by the *syngo*.via RT Image Suite to generate an sCT dataset in a few minutes (Fig. 2). Bones are rendered in the sCT image set using a multi atlas-based algorithm, so the three lowest lumbar vertebrae must be scanned during the sequence acquisition.

4. Treatment planning

A VMAT treatment plan was optimized using a Halcyon system (V2.0) with 6 MV flattening filter-free beam and Eclipse V15.6. Later, the sCT image and pCT image are registered rigidly and the structures and beam configurations are transferred to the sCT image. On the sCT image, the treatment plan is re-calculated, without new optimization.

5. Treatment and image guided radiotherapy

5.1 Halcyon with iCBCT (online matching)

For IGRT, the Halcyon linear accelerator uses daily CBCT with iterative image reconstruction (iCBCT) and slice thickness of 2 mm. A treatment session without imaging before dose application is not possible with this system.

1 Patient positioning in an MRI device using MRI compatible positioning aids: flat table top with knee immobilization device to reproduce the patient positioning from the simulation to the treatment, in this case using the Halcyon.

[2]The information shown herein refers to products of a 3rd party, which are their regulatory responsibility. Please contact the 3rd party for further information.

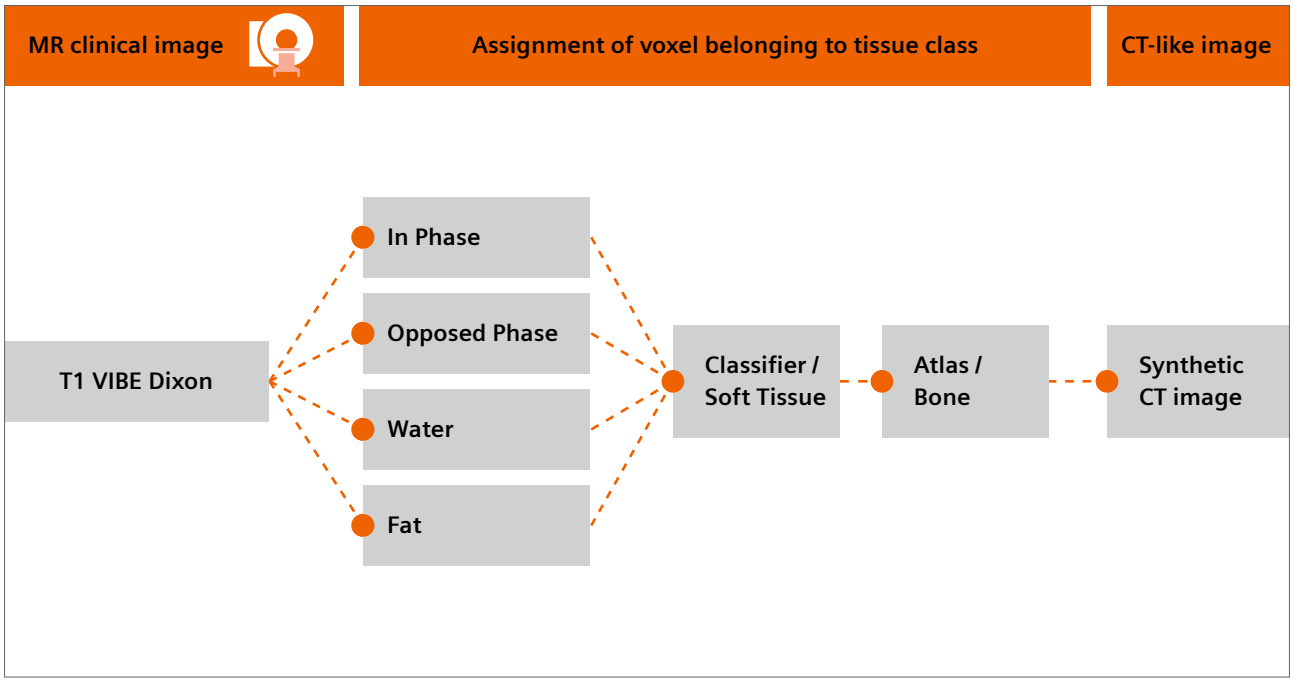

2 The synthetic CT algorithm for the pelvis, from image acquisition to synthetic CT image generation.

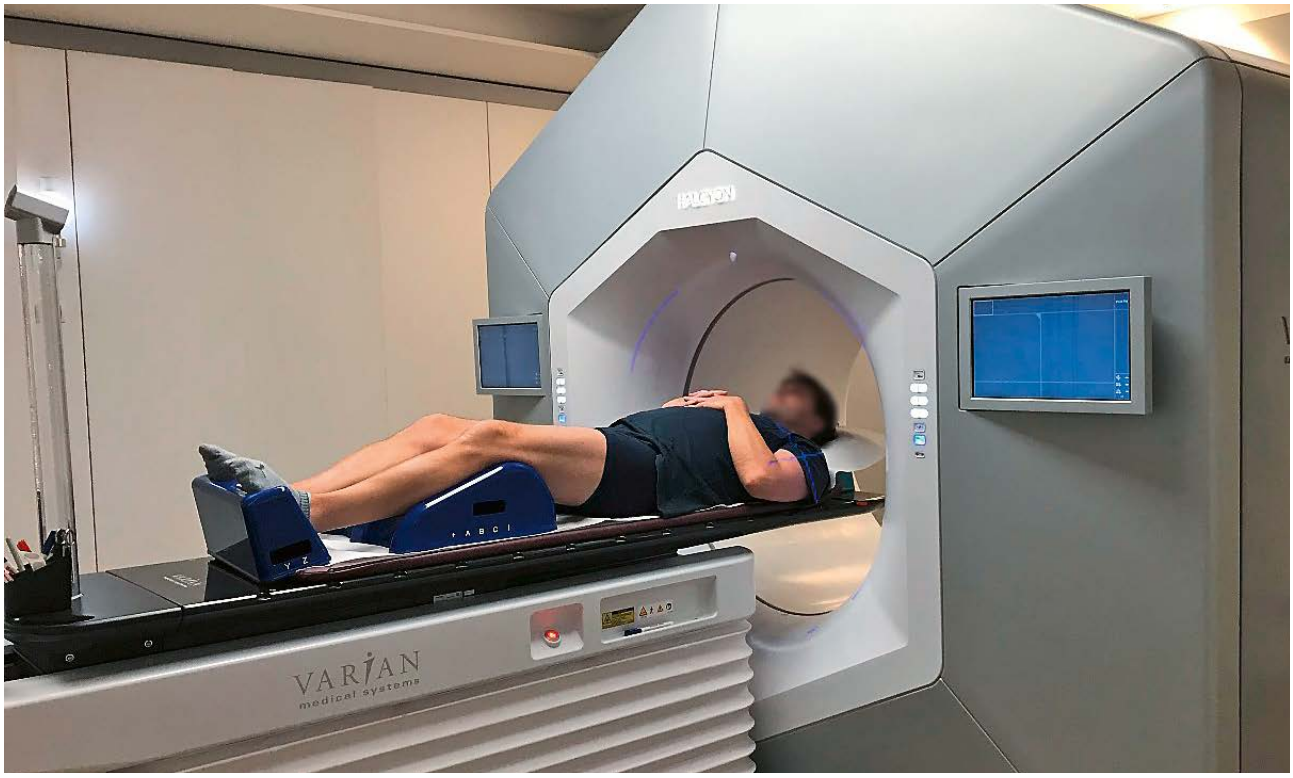

3 Patient positioning on the Halcyon.

5.2 Offline matching

In the implementation phase, each CBCT image is registered offline with the pCT and sCT images (Siemens and Spectronic). Registration is based on intensity differences and a pixel-based similarity optimization. For this auto-registration, a region including the PTV and a margin of 2 cm was selected (Fig. 4). To calculate translations in x-, y- and z-directions, the following equation was used:

$$\Delta\vec{V} = \Delta\vec{V}_{CBCT/pCT} - (\Delta\vec{V}_{CBCT/sCT} + \Delta\vec{V}_{pCT/sCT})$$

where the term $\Delta\vec{V}_{pCT/sCT}$ expresses the intrinsic offset between pCT and sCT images.

In order to perform this analysis analog to the clinical work, image registration was limited to translations, so rotation, pitch, and roll were not considered.

6. Quality assurance

Currently there is no official guideline for quality assurance (QA) for MRI systems used for radiotherapy planning.
To measure geometric distortions in MRI, the GRADE Phantom (Spectronic) was used. As result of the analysis, a PDF is generated with a 3D overview of the distortion in a clinically relevant scan volume (Fig. 5).

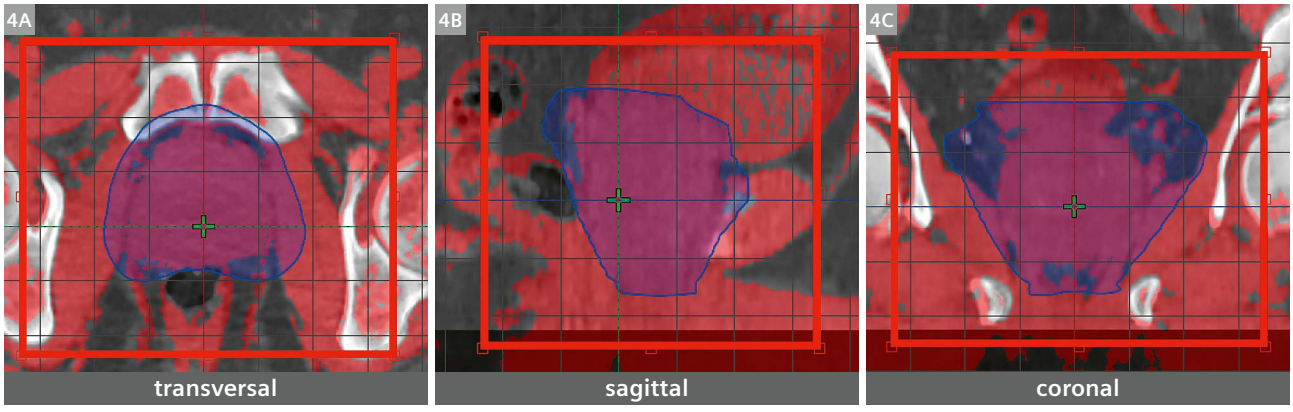

4 Example of image registration between CBCT images and CT images using soft tissue. The contoured PTV is in blue and the soft tissue used for the auto-registration algorithm is in red. The red line defines the volume of interest (VOI) used for the registration.

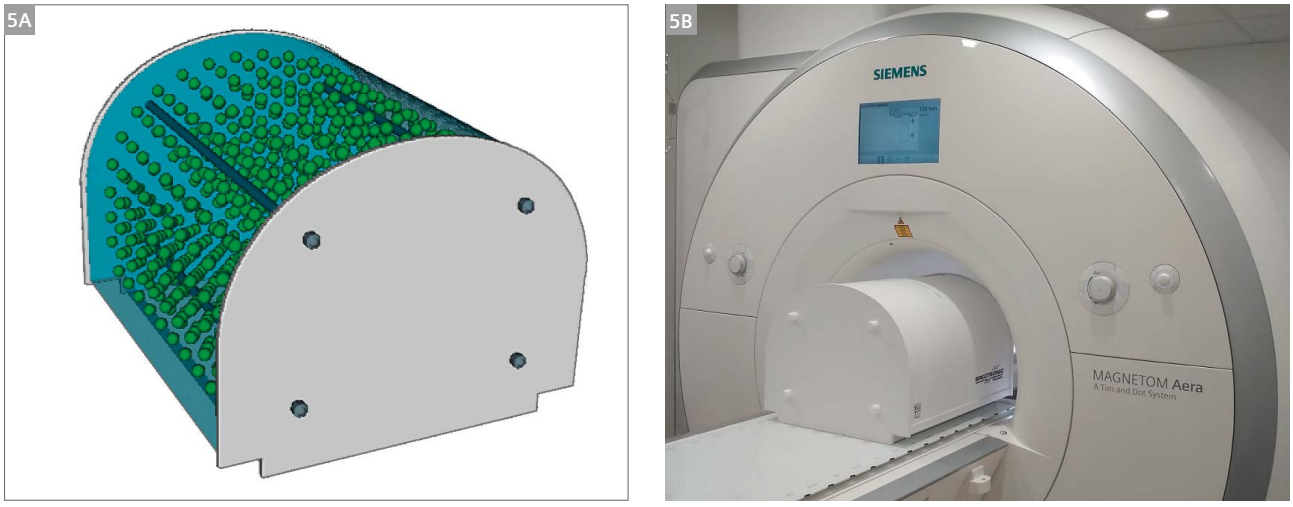

5 GRADE phantom from Spectronic, used to measure geometrical distortion. **(5A)** Image of the phantom. **(5B)** Phantom on the scanner allowing the measurement of geometric distortion in the entire scan field.

Results

Figure 6 shows an example of the results from the different sCT generation methods. The solution from Spectronic with its continuous Hounsfield units (HU) distribution is similar to a planning CT image whereas the Siemens solution uses a discrete HU distribution: Air (-1000 HU), fat (-75 HU), water (0 HU), spongy bone (204 HU) and cortical bone (1170 HU) (Fig. 6). The soft tissue of bladder, rectum and prostate is assigned 0 HU, like water. The sCT images from Spectronic use different HU values for different soft tissues, in analogy to pCT images.

Dose distributions

Different therapy concepts regarding the total dose were used during this study. For comparison reasons, the calculated plans were all normalized to the mean PTV dose and only relative dose deviations were considered.

In Figure 7, mean dose differences of the 15 patients are represented using a boxplot diagram, showing the results for the following OARs: rectum, bladder, and right- and left femoral head. The plot gives the difference between the calculated dose based on the sCT (Spectronic) and pCT (left box); and between the calculated dose based on the sCT (Siemens) and pCT (right box). The total mean difference is below 2%.

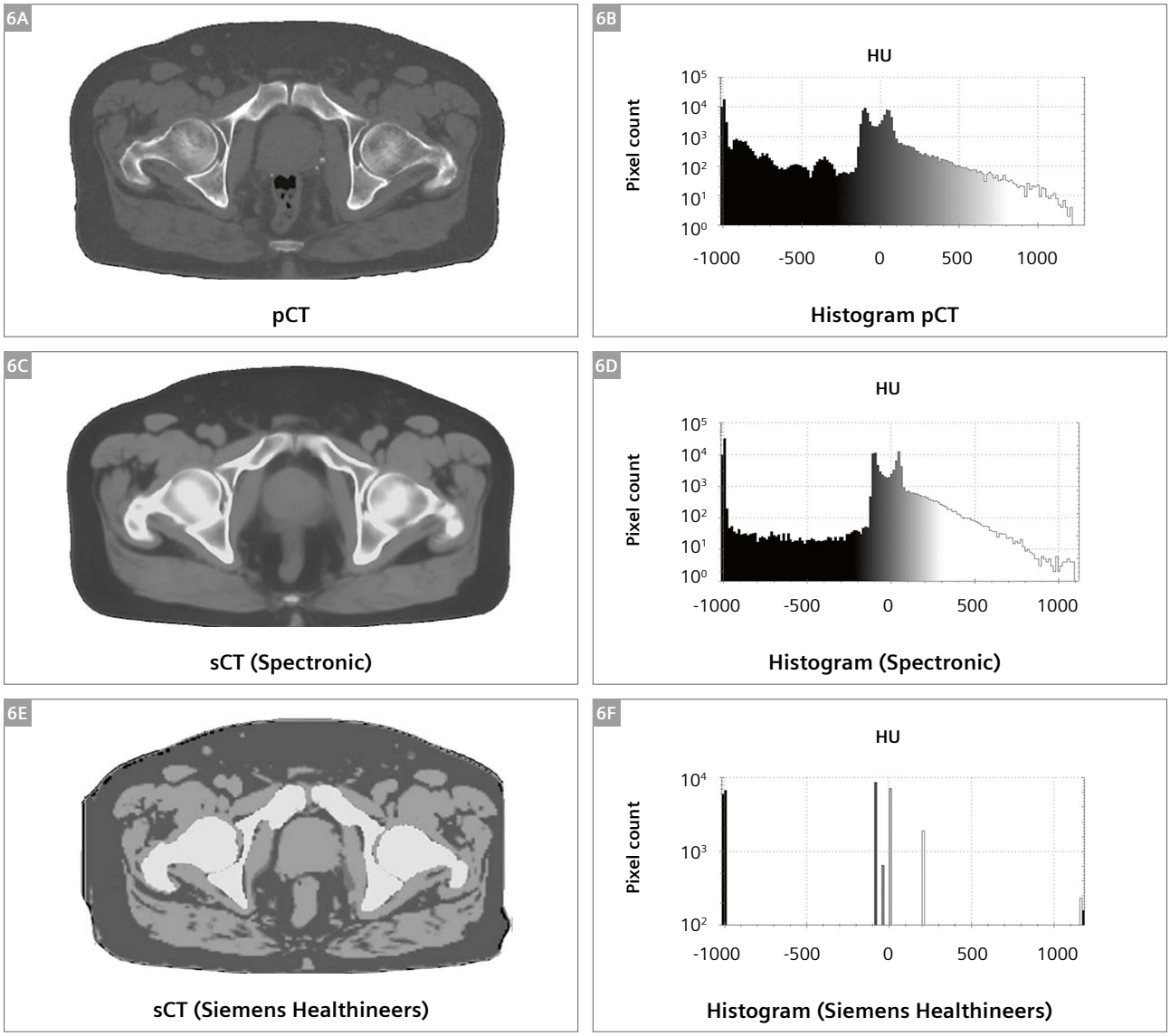

6 Examples of pCT (6A), sCT (Spectronic: 6C) and sCT (Siemens: 6E) representation including HU surface histogram (pCT: 6B; Spectronic: 6D; Siemens: 6F) of the shown cross-sectional images. The HU histograms of the pCT and the sCT (Spectronic) have a continuous spectrum from -1000 to 1210 HU and -1000 to 1071 HU, respectively. The HU histogram of the sCT (Siemens) has discrete values.

Offline matching

For both manufacturers, we evaluated translations after offline IGRT between CBCT/pCT and CBCT/sCT of 15 patients with a total of 513 CBCTs. In Figure 8, each point represents the deviation in one-dimensional direction from the registration (PTV + 2 cm, see Figure 4) between the CBCT and the respective pCT (vertical axis) and between CBCT and the respective sCT (horizontal axis). Considering all one-dimensional directions as independent parameters the correlation between sCT (Spectronic) and pCT images has a coefficient of determination of $R^2 = 0.895$. The correlation between sCT (Siemens) and pCT has a coefficient of determination of $R^2 = 0.851$. In the lateral (x) direction both sCT solutions show best correlations to CBCT compared to the CT (considered the gold standard).

For Spectronic, the worst correlation is in the z-direction whereas with the Siemens solution the lowest correlation is in the y-direction. Analyzing the registrations between CBCT and pCT images, 94% of the one-dimensional translations in the three directions are smaller than 10 mm. For registrations between sCT (Spectronic) and sCT (Siemens) respectively with CBCT images, 95% of the translations are smaller than 10 mm. The maximum difference between CBCT and pCT is 1.9 ± 5.2 mm in longitudinal direction (z), between CBCT and sCT (Spectronic) −2.5 ± 5.6 mm in vertical direction (y) and between CBCT and sCT (Siemens) 1.2 ± 5.5 mm in longitudinal direction.

The calculated translations between pCT and sCT differ significantly ($p < 0.001$) in all spatial directions, but they do not exceed 1 mm on average (Figure 9).

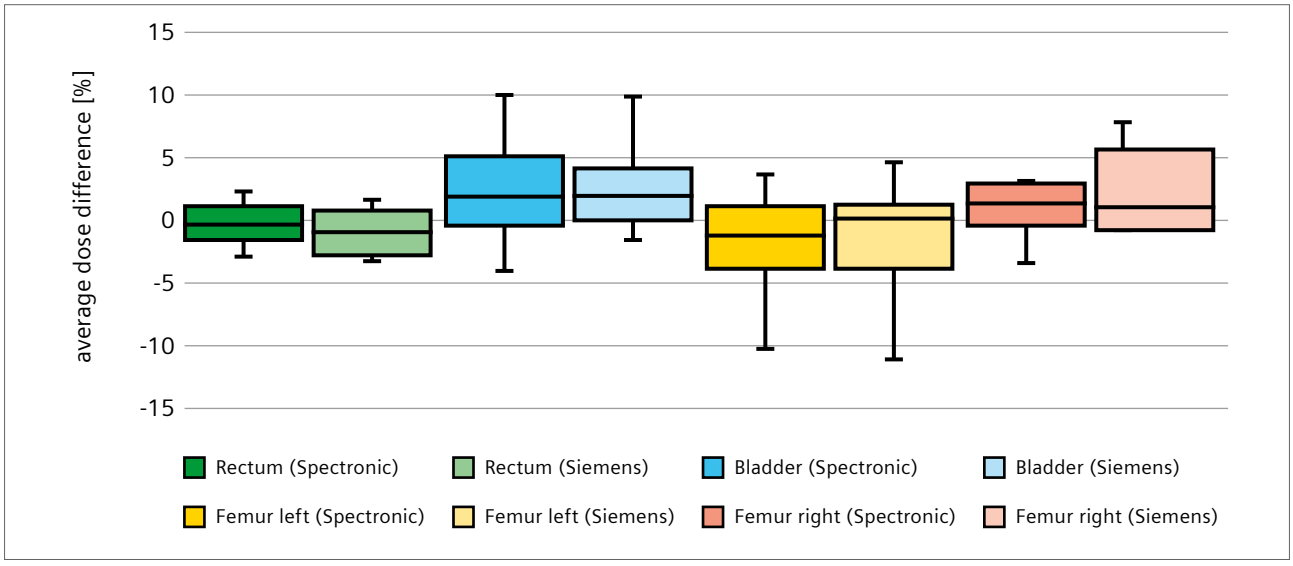

7 Boxplots of the mean dose difference of considered OARs. Representation of the dose differences to pCT, each in comparison to sCT.

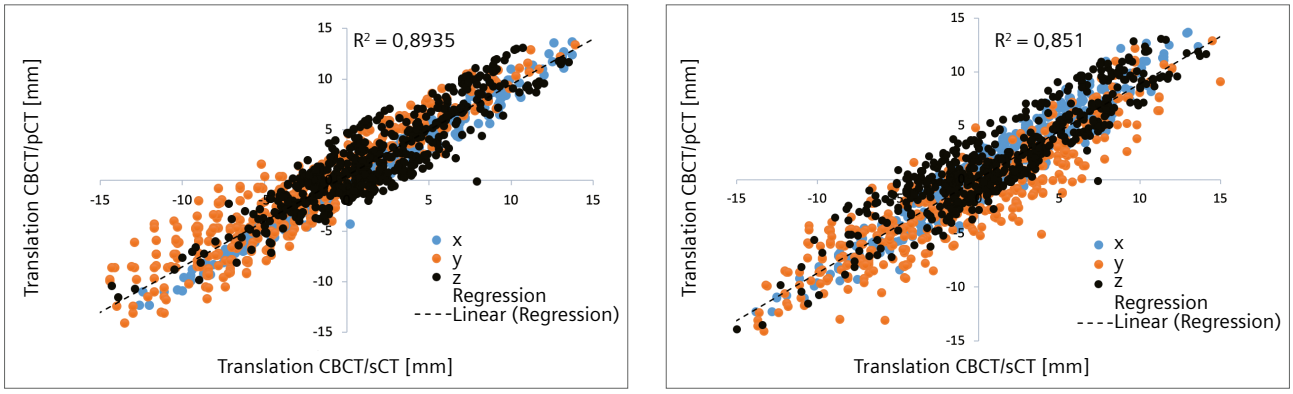

8 Scatterplot showing the translations from CBCT to pCT and from CBCT to sCT, for Spectronic (left) and Siemens (right) (n = 513 CBCTs). Estimations of the coefficient of determination considering all directions as independent values. Each direction is represented by a different color: blue = x, lateral; orange = y, vertical; black = z, longitudinal.

Discussion

In order to integrate the MR-only workflow into our clinical routine we had to develop a new CarePath (ARIA, Varian). For this, the existing workflow has been extended by adding the MRI simulation, including the sCT generation, as new task. This modified workflow comprises the pCT scan acquisition, followed by MRI acquisition when the MRI scanner was available. Afterwards, the standard clinical workflow was carried out. During the validation phase of this study, pCT images were used as basis for contouring, dose calculation, and IGRT. In the analysis, the results from sCT are compared with pCT as a reference.

The MR-only workflow eliminates the error introduced in the standard MR/CT workflow when doing image registration. Patient positioning during CT and MRI acquisition may be different. Moreover, scans are taken at different times, which can produce different internal geometry (for example bladder filling).

The standard simulation timeslot required for MR only is 45 minutes, independent of the chosen solution for sCT generation. The sequences required for sCT generation and

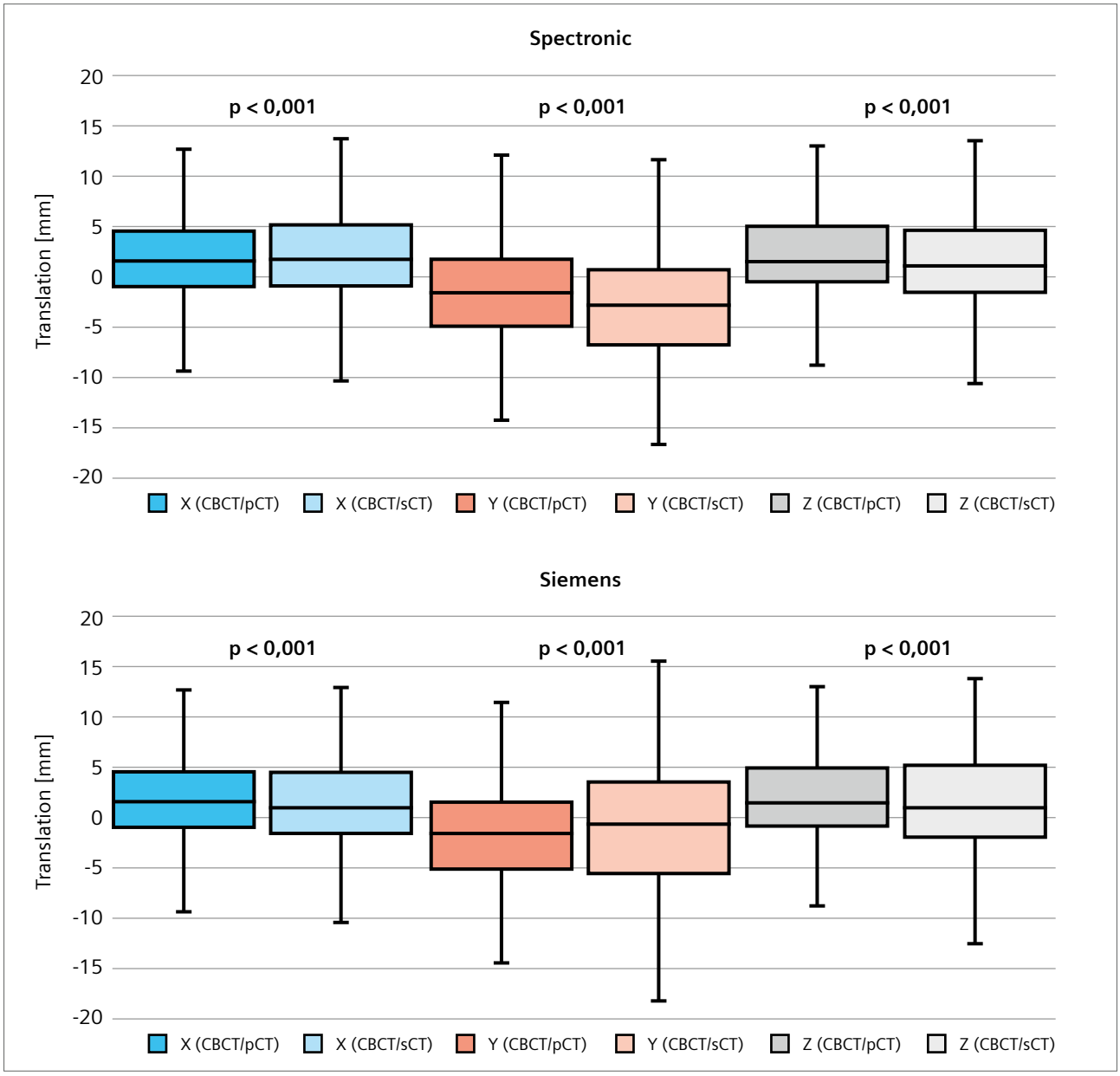

9 Boxplots of the translations of the CBCT registration to pCT, sCT (Spectronic) and sCT (Siemens). blue = x-direction, orange = y-direction, grey = z-direction.

also the diagnostic images for staging are taken at this time. If diagnostic images are already available, the timeslot is shortened to 20 minutes to acquire T2- and T1-Dixon sequences for contouring, and generate sCT images. The advantage of the quick T1-Dixon sequence from the Siemens solution is reduced when considering that a T2 sequence is normally needed for contouring. However, an important advantage of the quick acquisition is that motion artifacts are less prominent compared with those from a long sequence acquisition for sCT generation.

All 15 patients included in the implementation phase received a daily image-guided radiotherapy treatment in the prostate region at the Halcyon linear accelerator. A total of 513 CBCT images were compared with pCT and sCT images to calculate the translation. The values were significantly different when comparing the results from pCT (reference) images to the results from sCT images. The correlations (R^2 = 0.85–0.89) from CBCT/pCT and CBCT/sCT images demonstrate the difficulty when comparing the translation values from pCT and sCT images because of changes in geometry between pCT and MRI (sCT) scans taken at different times. The mean differences are smaller than 1.1 mm, and therefore not clinically relevant for daily IGRT on the Halcyon. They are, moreover, in accordance with already published studies [4].

IGRT based on sCT can therefore be performed on the Halcyon-System and allows the replacement of the conventional workflow using pCT as reference imaging for online matching. For the considered OARs the dose calculations based on sCT image sets from Siemens and

Spectronic show small mean differences and dose distributions.

The GRADE Phantom, adapted to MRI, allows to scan a large field of view, comparable to the field of view used for a pelvis patient. The mean distortion value measured in a clinically relevant field of view (150–200 mm from magnet isocenter) is 0.76 mm.

Conclusion

The MR-only workflow with the 1.5T MAGNETOM Aera has been successfully implemented. High contrast images for prostate contouring, and the immediate availability of the radiological report integrated in the ARIA OIS are helpful features that will lighten the daily workload in a busy clinical environment. The daily IGRT using the sCT image generated with the solution either from Siemens or Spectronic as reference CT can be performed on the Halcyon-system and allows the replacement of the conventional workflow using a pCT. The "pay-per-use"-model offered by Spectronic allows costs to be assigned to patients. The advantage of a license-based model as offered by Siemens is the unlimited and real-time availability of sCT.

References

1 Robert Koch Institute, Society of Epidemiological Cancer Registries in Germany, editors. Cancer in Germany for 2015/2016, 12th edition. Berlin, 2019.

2 Nyholm T, Nyberg M, Karlsson MG, Karlsson M. Systematisation of spatial uncertainties for comparison between a MR and a CT-based radiotherapy workflow for prostate treatments. Radiat Oncol. 2009; 4(1): 54. doi:10.1186/1748-717X-4-54.

3 Siversson C, Nordström F, Nilsson T, Nyholm T, Jonsson J, Gunnlaugsson A, Olsson LE. MRI only prostate radiotherapy planning using the statistical decomposition algorithm. Med. Phys. 2015; 42(10): 6090-6097. doi:10.1118/1.4931417.

4 Chen S, Quan H, Qin A, Yee S, Yan D. MR image-based synthetic CT for IMRT prostate treatment planning and CBCT image-guided localization. J Appl Clin Med Phys. 2016; 17(3): 236–245. doi:10.1120/jacmp. v17i3.6065.

Contact

Mandy Zimmermann M.Sc.
Medical Physics
Radiologische Allianz Hamburg
Mörkenstraße 47
22767 Hamburg
Germany
Tel.: +49 (40) 325552-598
mandy.zimmermann@radiologische-allianz.de

Left to right: M.Sc. Marcello Sabatino, Dr. Matthias Kretschmer, M.Sc. Mandy Zimmermann, Dr. Christian Giro

A Fully Automated, End-to-End Prostate MRI Workflow Solution Incorporating Dot, Ultrashort Biparametric Imaging and Deep-Learning-based Detection, Classification, and Reporting

David J. Winkel, M.D.[1]; Robert Grimm, Ph.D.[2]; Thomas Benkert, Ph.D.[2]; Berthold Kiefer, Ph.D.[2]; Daniel T. Boll, M.D.[1]

[1]Department of Radiology, University Hospital Basel, Switzerland
[2]MR Applications Predevelopment, Siemens Healthineers, Erlangen, Germany

Introduction

For more than a decade, magnetic resonance imaging (MRI) has been established as a powerful tool for prostate cancer diagnosis. The PROMIS study has demonstrated that prostate MRI is a suitable triage tool for biopsy-naïve men, reducing the number of unnecessary biopsies by a quarter while improving the detection of clinically significant cancer [1]. The PRECISION study randomized patients to either systematic biopsies or MRI; with no biopsy if MRI was negative, and targeted biopsy if MRI was positive. Targeted biopsies guided by MRI detected significantly more clinically significant cancers while reducing the number of clinically insignificant cancers [2]. Because of these findings, MRI for prostate cancer diagnosis has been integrated into established guidelines [3].

Increasing demand for prostate MRI examinations can be expected, as the incidence of prostate cancer increases with age and life-expectancy in developed countries is rising. Furthermore, prostate MRI has been discussed in the literature as a screening tool, similar to breast cancer screening [4]. However, several limitations need to be addressed in order to prepare for this increasing prostate MRI workload. Variation in MRI data acquisitions could be reduced [5]. Another limitation is the relatively long acquisition time of multiparametric MRI examinations (mpMRI) employing T2-weighted (T2w), diffusion-weighted imaging (DWI) and dynamic-contrast enhanced (DCE) MRI. Several studies have shown that an approach without DCE MRI, called biparametric MRI (bpMRI), yields comparable results to mpMRI of the prostate [6]. Potentially even more important topic is the varying interpretation performance based on the expertise level. However, even among expert radiologists, agreement on prostate cancer classification based on established guidelines is imperfect [7, 8].

This all points to a clear need for

1. Efficient, reproducible, and robust data acquisition workflow
2. Optimized and fast sequence design
3. Automated detection, classification, and reporting workflows in prostate MRI examinations

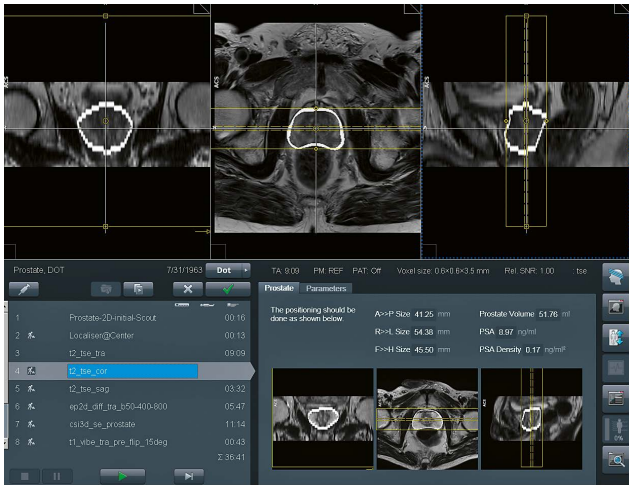

1 Image acquisition using the Prostate Dot Engine[1] including automated prostate contour detection, prostate centering, field of view adaption and three-dimensional correction of spatial axes.

[1]*Work in progress: the application is currently under development and is not for sale in the U.S. and in other countries. Its future availability cannot be ensured.*

This is a chain of independent, yet highly interlinked stages. Well-registered and reformatted images with reproducible high image quality are a key prerequisite for optimal and reproducible artificial intelligence-based analyses.

In this article, we outline an end-to-end solution that addresses all the limitations above, incorporating day optimizing throughput (Dot), ultrashort bpMRI and deep-learning-based lesion detection, classification and reporting. We present two example cases using the proposed workflow in order to illustrate its feasibility.

Material and methods

Prostate Dot Engine

The Prostate Dot Engine[1] is a prototype software tool designed to provide a fast, robust, and standardized image acquisition workflow. After acquiring the Turbo-Spin Echo (TSE) scout, the Prostate Dot automatically centers the prostate in the field of view, adapts the size of the field of view and performs a three-dimensional correction of spatial axes. Slices can be aligned either strictly orthogonal or automatically defined by the orientation of the urethra, i.e., perpendicular to the urethra for the axial planes. Furthermore, the prostate is segmented for standardized volume assessment. After coil placement, the Dot workflow does not require further adaptations by technicians, and it allows interruptions and corrections of the scan process at any time. A screenshot of the Prostate Dot Engine can be found in Figure 1.

Sequence specifications

The biparametric protocol consists of a T2-weighted turbo spin-echo (TSE) pulse sequence in axial, sagittal and coronal orientations and an improved single shot DWI EPI sequence (ZOOMit^{PRO}, Siemens Healthcare, Erlangen, Germany) with consecutive computation of the apparent diffusion coefficient. Unlike other DWI techniques, ZOOMit^{PRO} magnifies the prostate (in the phase-encoding direction) and is free of infolding artifacts. Either a smaller quadratic FOV or only a reduced FOV in the phase-encoding direction ('stripe') is excited (see Figure 2A). As there is no signal from the non-excited regions, only the small stripe needs to be encoded (see Figures 2B, C). That means the encoding time can be decreased while maintaining spatial resolution, or the spatial resolution can be increased, or a combination of the two. Furthermore, decreased encoding time reduces spatial distortion.

Prostate AI

The output of the Prostate Dot Engine goes into the AI prototype (Prostate AI[1], Siemens Healthcare, Erlangen, Germany) for fully automatic prostate lesion detection, classification and reporting.

As illustrated in Figure 3, Prostate AI contains two parts:

1. A preprocessing pipeline
2. A component for lesion detection and classification, based on deep learning

The preprocessing pipeline takes the acquired bpMRI sequences and generates the required well-formatted and transformed data volumes. From the DWI series, a logarithmic extrapolation method is adopted to compute a new DWI volume with *b*-value of 2000 s/mm^2. This step

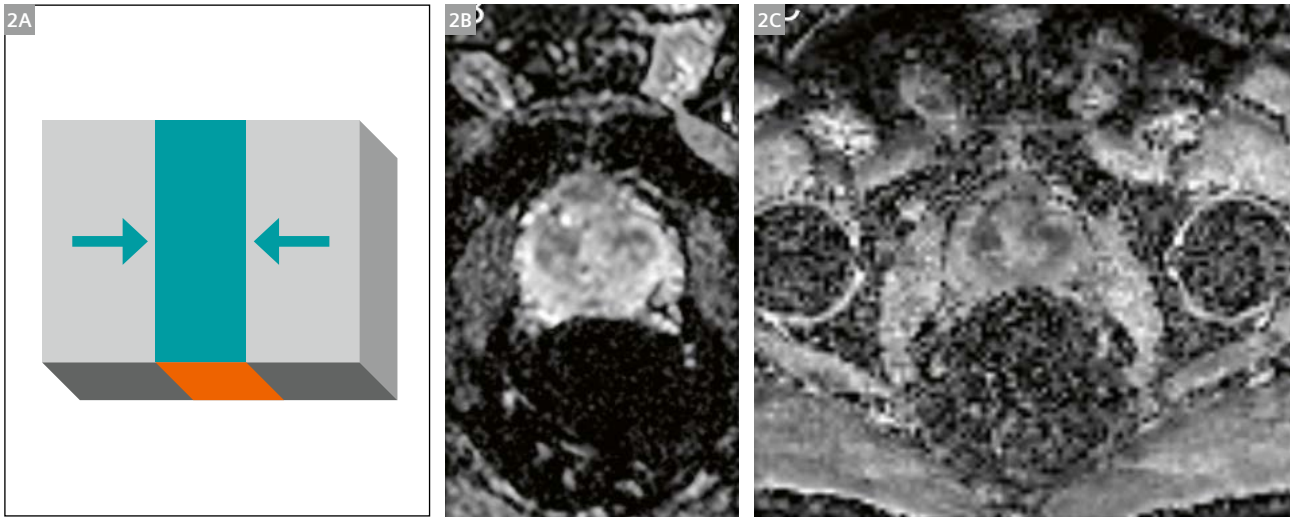

2 Single-shot DWI EPI sequence (ZOOMit^{PRO}) with image examples from one study object: **(2A)** reduced FOV in phase-encoding direction (blue stripe); **(2B)** resulting image in comparison to **(2C)** the conventional RESOLVE technique.

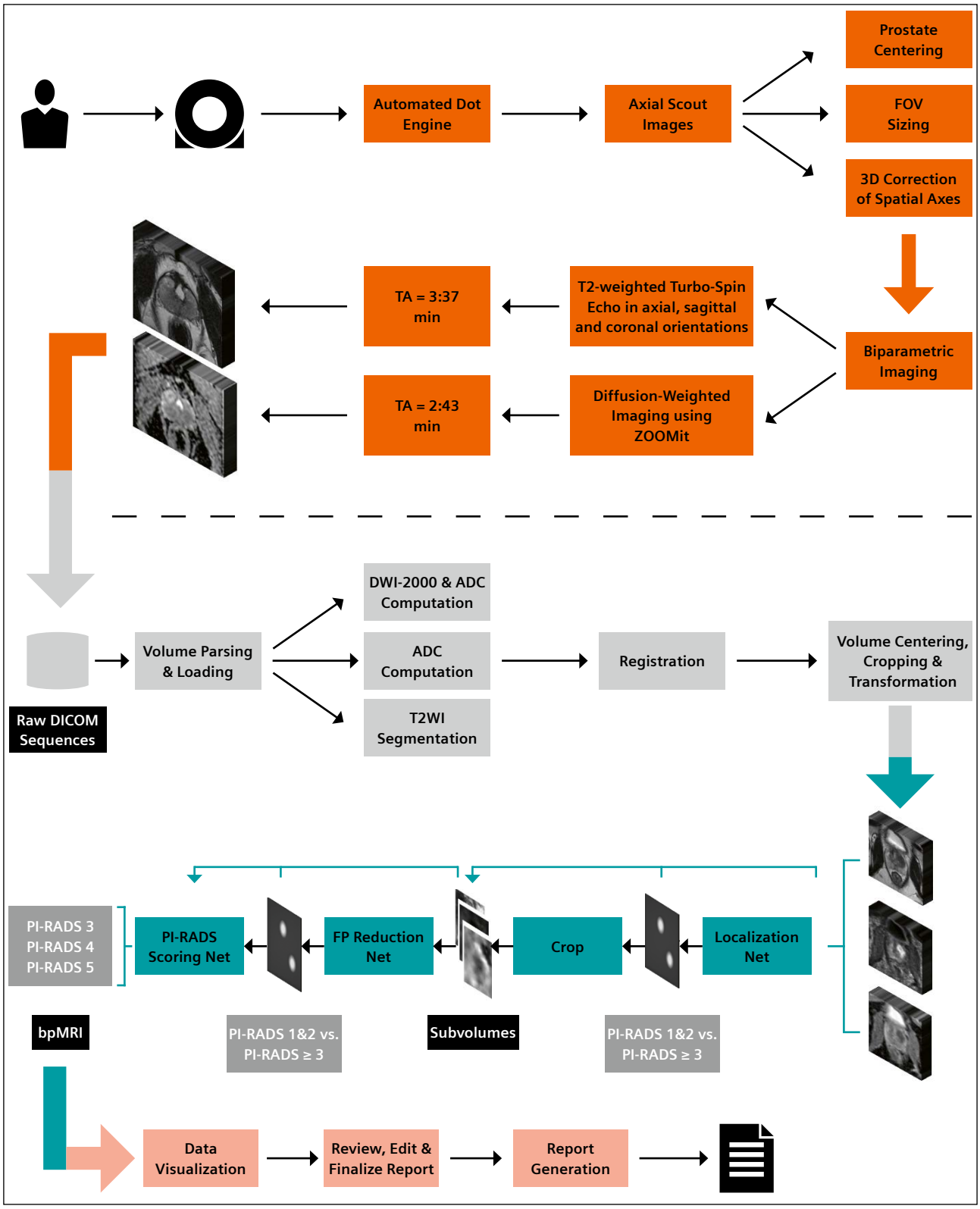

3 Image acquisition workflow using the automated Prostate Dot Engine and biparametric imaging (orange); deep learning architecture with preprocessing pipeline (gray); deep learning-based lesion detection and classification component (blue).

Dot = day optimizing throughput, FOV = field of view, 3D = three-dimensional, TA = time of acquisition, DICOM = Digital Imaging and Communications in Medicine, ADC = apparent diffusion coefficient, FP = false positive, PI-RADS = Prostate Imaging Reporting- and Data System

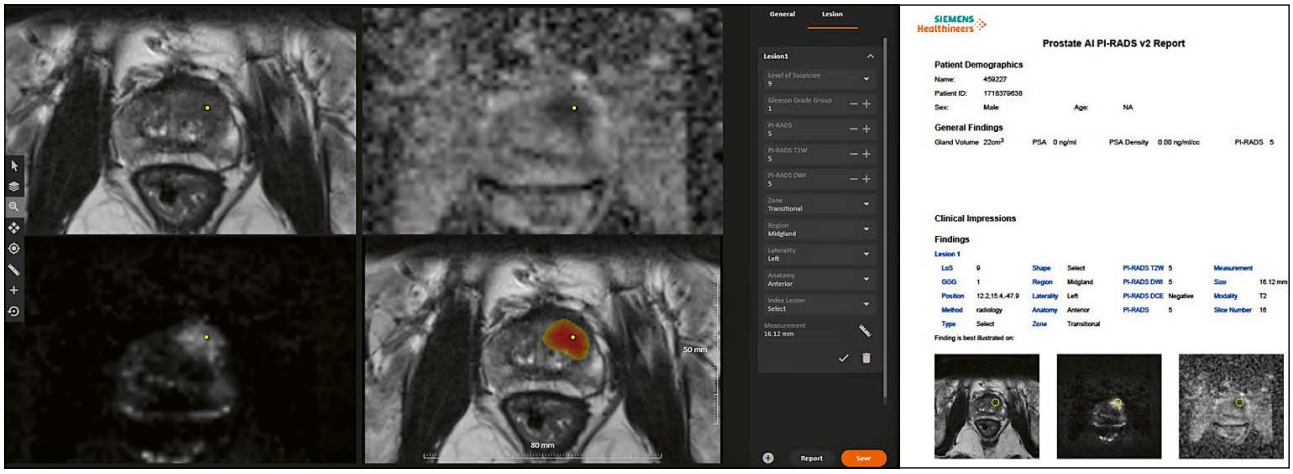

4 Data visualization platform with the T2w images, ADC map, and high *b*-value image as well as the T2w image overlaid with the AI-generated heatmap (in red and yellow). Prostate AI automatically detected the suspect lesion in the transition zone (TZ, yellow dot) and pre-populated all relevant information according to current PI-RADS guidelines. Next, a machine-readable report based on this information is generated.

can eliminate the *b*-value variances among the datasets and also improve lesion detection performance [10]. Also, apparent diffusion coefficient (ADC) maps are computed. Next, whole-organ gland segmentation is performed on the T2w volume using a learning-based method as presented in Yang et al. [11]. After segmentation, a rigid registration is conducted to align T2w and DWI images. The preprocessing pipeline can eliminate both geometric and intensity variances across sequences and patient studies.

Prostate AI then automatically detects clinically relevant lesions and classifies each detected lesion according to PI-RADS categories. This is achieved by a sequence of coupled deep neural networks that are trained separately. First, a fully convolutional localization net is able to generate a semantic lesion candidate heatmap (see Figures 5 and 6); then a subvolume-based false positive reduction net further improves detection accuracy by removing the false positives; finally another sub-volume-based PI-RADS scoring net stages the level of malignancy for each detection according to PI-RADS categories.

In a last step, Prostate AI displays the detection and classification results on a dedicated platform. As the ability of the interpreting radiologist to accept or reject AI-based findings has been identified as a prerequisite for adoption of these techniques [12], these capabilities have been implemented. The user is then able to create a machine-readable report with all relevant information for the referring physician (see Figure 4). This report can be sent to the local RIS/PACS system.

Cases

Case 1

Figures 5A-D demonstrate a lesion in the right midgland PZpl/PZa of a 62-year-old man, with a maximum diameter of 30.2 mm and a mean ADC-value of 758 µm²/s. Prostate AI detected the lesion and assigned a PI-RADS 5 category. Biopsy results revealed a Gleason 4+3 = 7 pattern.

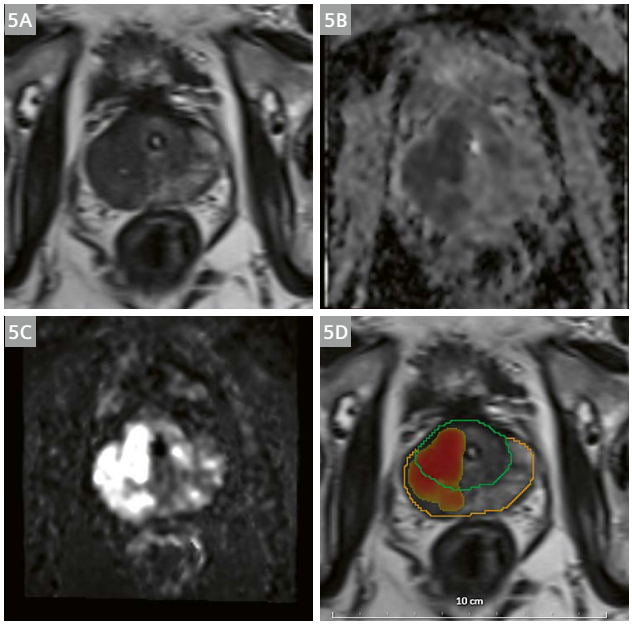

Case 2
Figures 6A-D demonstrate a lesion in the left apical PZpl of a 51-year-old man, with a maximum diameter of 10.2 mm and a mean ADC-value of 961 µm²/s. Prostate AI detected the lesion and assigned a PI-RADS 4 category. Biopsy results revealed a Gleason 3+3 = 6 pattern.

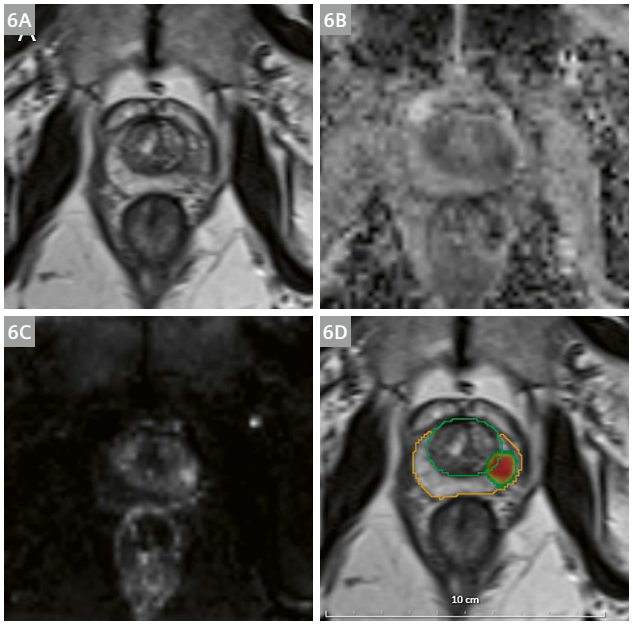

Conclusion

In this article, we outlined an end-to-end concept to allow a standardized workflow with a reproducible and fast data acquisition with optimized imaging sequences and an AI-empowered data analysis including automated detection, classification and reporting of suspicious lesions in biparametric prostate MRI examinations.

Reproducible and fast data acquisition concepts are not only contributing to a standardized reporting performed by human readers but would also help artificial intelligence-based solutions to reliably process input data. Preliminary results from a study conducted at the University of Innsbruck in Austria including 50 patients referred for a prostate MRI examination, compared the tilting angle of the auto-alignment of the Prostate Dot Engine against axes determined manually by an experienced radiologist, serving as the reference-standard. The investigators were able to show a mean ± SD deviation of the tilting angle of 5.5 ± 4.4 degrees (Ch. Kremser, W. Judmaier, Med. Uni Innsbruck, unpublished results). However, to date, there is no study investigating workflow differences, such as time-saving metrics, between Dot-guided and conventional, technician-guided workflows. Those studies are currently planned, and their results will contribute to reveal the value of Dot engines in clinical routine.

Concerning the use of abbreviated protocols consisting of T2-weighted and DWI only – so-called biparametric prostate MRI – several studies [6, 13, 14] have shown comparable results as obtained with conventional, mpMRI protocols including DCE-MRI. We added another component to our suggested workflow, that is performing DWI with the ZOOMit^{PRO}. As shown in Figure 2, ZOOMit^{PRO} uses a reduced FOV in the phase-encoding direction compared with either standard single shot DWI EPI or RESOLVE (REadout Segmentation Of Long Variable Echo trains). The resulting decreased acquisition time can be invested in a superior spatial resolution. Future studies are needed to systematically investigate differences between different types of DWI acquisition schemes compared to the ZOOMit^{PRO} technique.

The last component in our workflow is the use of AI-based lesion detection and classification. Schelb et al. [15] used the input from T2w sequences and DWI to train a deep learning algorithm (Unet) on the histopathological outcome, serving as ground truth. They were able to show that this algorithm achieved a similar performance to human readers using the PI-RADS assessment score. Cao et al. [16] used the input of mpMRI images to build a convolutional neural network trained on histopathological data and used this algorithm to detect suspicious lesions and to predict the Gleason score. The results were promising, with a high sensitivity for lesion detection – comparable to expert human readers – and a high classification performance with regards to clinically significant cancer. However, the usefulness of these algorithms needs to be proven in larger multi-reader, multi-case (MRMC) studies, systematically examining their influence on interpretation performance and speed, with and without those solutions.

We have identified a need to re-structure existing prostate MRI workflows, as patient or – in case of screening approaches – participant throughput is expected to increase. In our vision, current workflows need more reliable, reproducible and fast data acquisition steps. Furthermore, recent research has shown that deep learning algorithms can compete with human intelligence in prostate MRI reporting. We outlined a possible end-to-end solution and demonstrated its feasibility with two case examples. Future research will investigate what impact the individual components or the combination of those components will have on the future of prostate MRI.

References

1 Ahmed HU, El-Shater Bosaily A, Brown LC, et al. Diagnostic accuracy of multi-parametric MRI and TRUS biopsy in prostate cancer (PROMIS): a paired validating confirmatory study. Lancet. 2017;389:815–822. https://doi.org/10.1016/S0140-6736(16)32401-1

2 Kasivisvanathan V, Rannikko AS, Borghi M, et al. MRI-Targeted or Standard Biopsy for Prostate-Cancer Diagnosis. N Engl J Med. 2018;378:1767–1777. https://doi.org/10.1056/NEJMoa1801993

3 EAU Guidelines. Presented at the EAU Annual Congress Barcelona 2019. ISBN 978-94-92671-04-2.

4 Kim SJ, Vickers AJ, Hu JC. Challenges in Adopting Level 1 Evidence for Multiparametric Magnetic Resonance Imaging as a Biomarker for Prostate Cancer Screening. JAMA Oncol. 2018;4:1663–1664. https://doi.org/10.1001/jamaoncol.2018.4160

5 Padhani AR, Barentsz J, Villeirs G, et al. PI-RADS Steering Committee: The PI-RADS Multiparametric MRI and MRI-directed Biopsy Pathway. Radiology. 2019;292:464–474. https://doi.org/10.1148/radiol.2019182946

6 Weiss J, Martirosian P, Notohamiprodjo M, et al. Implementation of a 5-Minute Magnetic Resonance Imaging Screening Protocol for Prostate Cancer in Men with Elevated Prostate-Specific Antigen before Biopsy. Invest Radiol. 2018;53:186–190. https://doi.org/10.1097/RLI.0000000000000427

7 Weinreb JC, Barentsz JO, Choyke PL, et al. PI-RADS Prostate Imaging - Reporting and Data System: 2015, Version 2. Eur Urol. 2016;69:16–40. https://doi.org/10.1016/j.eururo.2015.08.052

8 Rosenkrantz AB, Ginocchio LA, Cornfeld D, et al. Interobserver Reproducibility of the PI-RADS Version 2 Lexicon: A Multicenter Study of Six Experienced Prostate Radiologists. Radiology. 2016;280:793–804. https://doi.org/10.1148/radiol.2016152542

9 Maas MC, Fütterer JJ, Scheenen TW. Quantitative evaluation of computed high b value diffusion-weighted magnetic resonance imaging of the prostate. Invest Radiol. 2013;48:779.

10 Rosenkrantz AB, Parikh N, Kierans AS, et al. Prostate Cancer Detection Using Computed Very High b-value Diffusion-weighted Imaging: How High Should We Go? Acad Radiol. 2016;23:704–711. https://doi.org/10.1016/J.ACRA.2016.02.003

11 Yang D, Xu D, Zhou SK, et al. Automatic Liver Segmentation Using an Adversarial Image-to-Image Network. In: Descoteaux M, Maier-Hein L, Franz A, et al (eds) Medical Image Computing and Computer Assisted Intervention – MICCAI 2017. Springer International Publishing, Cham. 2017; pp 507–515.

12 Padhani AR, Turkbey B. Detecting Prostate Cancer with Deep Learning for MRI: A Small Step Forward. Radiology. 2019;192012. https://doi.org/10.1148/radiol.2019192012

13 Kuhl CK, Bruhn R, Krämer N, et al. Abbreviated Biparametric Prostate MR Imaging in Men with Elevated Prostate-specific Antigen. Radiology. 2017;282:493–505. https://doi.org/10.1148/radiol.2017170129

14 Woo S, Suh CH, Kim SY, et al. Head-to-head comparison between biparametric and multiparametric MRI for the diagnosis of prostate cancer: A systematic review and meta-analysis. Am J Roentgenol. 2018;211:W226–W241. https://doi.org/10.2214/AJR.18.19880

15 Schelb P, Kohl S, Radtke JP, et al. Classification of Cancer at Prostate MRI: Deep Learning versus Clinical PI-RADS Assessment. Radiology. 2019;190938. https://doi.org/10.1148/radiol.2019190938

16 Cao R, Bajgiran AM, Mirak SA, et al. Joint Prostate Cancer Detection and Gleason Score Prediction in mp-MRI via FocalNet. IEEE Trans Med Imaging. 2019;38:2496–2506. https://doi.org/10.1109/TMI.2019.2901928

Contact

David J. Winkel, M.D.
Department of Radiology
University Hospital Basel
Spitalstrasse 21
4031 Basel
Switzerland
Tel.: +41 61 328 65 22
davidjean.winkel@usb.ch

Meet Siemens Healthineers

Siemens Healthineers: Our brand name embodies the pioneering spirit and engineering expertise that is unique in the healthcare industry. The people working for Siemens Healthineers are totally committed to the company they work for, and are passionate about their technology. In this section we introduce you to colleagues from all over the world – people who put their hearts into what they do.

Nuria Escobar Corral, Ph.D.

I was born and raised in Spain. I moved to Germany when I was 21, as part of the ERASMUS exchange program between European universities. It was supposed to just be for a year, but I ended up staying. After earning a degree in physics from Universidad de Valencia, Spain, I went on to work as a medical physicist in the Department of Radiotherapy at Uniklinik RWTH Aachen, Germany, from 2009 to 2017. During this time, I also earned my Ph.D. in a collaboration with the Department of Physics at RWTH Aachen University. In 2017, my family and I moved to Bamberg, where I spent 18 months working in the Department of Radiation Oncology at University Hospital Erlangen, before joining Siemens Healthineers in April 2019. In my role as a clinical and scientific specialist in imaging for radiotherapy, I work on topics involving the use of multimodality imaging in radiotherapy.

Forchheim, Germany

How did you first come into contact with MRI?
As a medical physicist in radiotherapy departments, I was in contact with MR images, but not with MR systems. Images were produced elsewhere, and we used them to support therapy planning. I was very impressed by the soft-tissue contrast MRI could achieve, which is especially useful for head and pelvis cases in radiotherapy. My first real contact with an MR system was when I joined Siemens Healthineers. I'm amazed at everything I've learned this past year, and at everything that MRI can offer to radiotherapy.

What do you find most fascinating about MRI?
That's a difficult question: The technology is so fascinating that it's hard to choose one thing. Compared to the classic CT radiotherapy world, for example, it's fascinating that you can measure different physical processes and obtain different images and therefore different clinical information, all in one measurement session. I'm also astonished at the contrast provided by MRI images. It enables clinicians to establish the boundaries between organs and tumors much more confidently. I would say that MRI reveals anatomical and physiological details that we could previously only guess from CT images. I'm also very interested in the possibilities presented by functional imaging for assessing treatments or even predicting treatment outcomes. It might also play an important role in dose painting in the future. Overall, MRI and radiotherapy are a recently married pair that are opening up a new world of possibilities for cancer treatment.

What do you find motivating about your job?
I see my role as a mediator between the MRI and radiotherapy worlds. They have different ways of working, and even a different language. And now that the use of MRI in radiotherapy is increasing so quickly, they are forced to understand each other. As a mediator, I must understand both MR and radiotherapy, and build the bridges that enable communication. I find this task very interesting, and the challenges associated with it are very motivating.

If you could do anything you wanted for a month, what would it be?
I'd probably spend some time performing measurements with our MR systems, learning all the information we can acquire from different sequences, and building my expertise for our software solutions.

Outside of work, you can usually find me with my two sons, reading a book, playing a board game, or riding a bike. I am very family oriented and I love travelling. So when we have free time, we visit my parents in Spain, or my parents-in-law in Brazil. I also love discovering new places with my husband and my kids. For example, we're traveling to Norway by car this summer and we're already excited about it.

Not for distribution in the US

On account of certain regional limitations of sales rights and service availability, we cannot guarantee that all products included in this brochure are available through the Siemens sales organization worldwide. Availability and packaging may vary by country and is subject to change without prior notice. Some/All of the features and products described herein may not be available in the United States.

The information in this document contains general technical descriptions of specifications and options as well as standard and optional features which do not always have to be present in individual cases, and which may not be commercially available in all countries.

Due to regulatory reasons their future availability cannot be guaranteed. Please contact your local Siemens organization for further details.

Siemens reserves the right to modify the design, packaging, specifications, and options described herein without prior notice. Please contact your local Siemens sales representative for the most current information.

Note: Any technical data contained in this document may vary within defined tolerances. Original images always lose a certain amount of detail when reproduced.

Siemens Healthineers Headquarters
Siemens Healthcare GmbH
Henkestr. 127
91052 Erlangen, Germany
Phone: +49 9131 84-0
siemens-healthineers.com

Published by Siemens Healthcare GmbH · Order No. A91MR-1100-110C-7600 · Printed in Germany · 8782 0420 ·

siemens.com/magnetom-world-rt